1

General Circulation of Planetary Atmospheres: Insights from Rotating Annulus and Related Experiments

Peter L. Read[1], Edgar P. Pérez[2], Irene M. Moroz[2], and Roland M. B. Young[1]

1.1. LABORATORY EXPERIMENTS AS "MODELS" OF PHYSICAL SYSTEMS

In engineering and the applied sciences, the term "model" is typically used to denote a device or concept that imitates the behavior of a physical system as closely as possible, but on a different (usually smaller) scale, possibly with some simplifications. The aim of such a model is normally to evaluate the performance of such a system for reasons connected with its exploitation for economic, social, military, or other purposes. In the context of the atmosphere or oceans, numerical weather and climate prediction models clearly fall into this category. Such models are extremely complicated entities that seek to represent the topography, composition, radiative transfer, and dynamics of the atmosphere, oceans, and surface in great detail. As a result, it is generally impossible to comprehend fully the complex interactions of physical processes and scales of motion that occur within any given simulation. The success of such models can only be judged by the accuracy of their predictions as directly verified (in the case of numerical weather prediction) against subsequent observations and measurements. Similar models used for climate prediction, however, are often comparable in complexity to those used for weather prediction but are frequently used as tools in attempts to address questions of economic, social, or political importance (e.g., concerning the impact of increasing anthropogenic greenhouse gas emissions) for which little or no verifying data may be available.

In formulating such models and interpreting their results, it is necessary to make use of a different class of model, the "conceptual" or "theoretical" model, which may represent only a small subset of the geographical detail and physical processes active in the much larger, applications-oriented model but whose behavior may be much more completely understood from first principles. To arrive at such a complete level of understanding, however, it is usually necessary to make such models as simple as possible ("but no simpler") and in geometric domains that may be much less complicated than found in typical geophysical contexts. An important prototype of such a model in fluid mechanics is that of dimensional (or "scale") analysis, in which the entire problem reduces to one of determining the leading order balance of terms in the governing equations and the consequent dependence of one or more observable parameters in the form of power law exponents. Following such a scale analysis, it is often possible to arrive at a scheme of mathematical approximations that may even permit analytical solutions to be obtained and analyzed. The well-known quasi-geostrophic approximation is an important example of this approach [e.g., see *Holton*, 1972; *Vallis*, 2006] that has enabled a vast number of essential dynamical processes in large-scale atmospheric and oceanic dynamics to be studied in simplified (but nonetheless representative) forms.

For the fundamental researcher, such simplified "conceptual" models are an essential device to aid and advance understanding. The latter is achievable because simplified, approximated models enable theories and hypotheses to be formulated in ways that can be tested (i.e., falsified, in the best traditions of the scientific method) against observations and/or experiments. The ultimate aim of such studies in the context of atmospheric and oceanic sciences is to develop an overarching framework that sets in perspective *all* planetary atmospheres and oceans, of which Earth represents but one set of examples [*Lorenz*, 1967; *Hide*, 1970; *Hoskins*, 1983].

[1]*Atmospheric, Oceanic & Planetary Physics, University of Oxford, Oxford, United Kingdom.*

[2]*Mathematical Institute, University of Oxford, Oxford, United Kingdom.*

Modeling Atmospheric and Oceanic Flows: Insights from Laboratory Experiments and Numerical Simulations,
First Edition. Edited by Thomas von Larcher and Paul D. Williams.

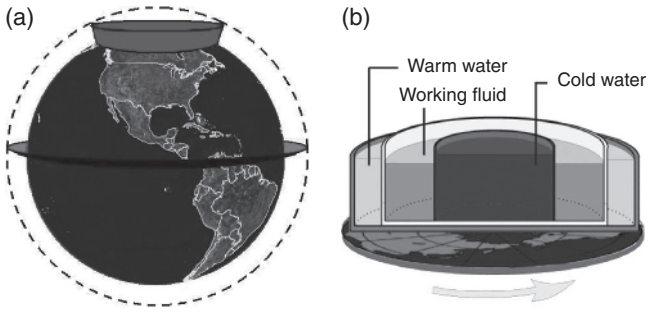

Figure 1.1. (a) Schematic diagram of a rotating annulus; (b) schematic equivalent configuration in a spherical fluid shell (cf. an atmosphere).

The role of laboratory experiments in fluid mechanics in this scheme would seem at first sight to be as models firmly in the second category. Compared with a planetary atmosphere or ocean, they are clearly much simpler in their geometry, boundary conditions, and forcing processes (diabatic and mechanical), e.g., see Figure 1.1. Their behavior is often governed by a system of equations that can be stated exactly (i.e., with no controversial parameterizations being necessary), although even then exact mathematical solutions (e.g., to the Boussinesq Navier-Stokes equations) may still be impossible to obtain. Unlike atmospheres and oceans, however, it is possible to carry out controlled experiments to study dynamical processes in a real fluid without recourse to dubious approximations (necessary to both analytical studies and numerical simulation). Laboratory experiments can therefore complement other studies using complex numerical models, especially since fluids experiments (a) have effectively infinite resolution compared to their numerical counterparts (though can only be measured to finite precision and resolution), (b) are often significantly less diffusive than the equivalent fluid, e.g., in eddy-permitting ocean models, and yet (c) are relatively cheap to run!

In discussing the role of laboratory experiments, however, it is not correct to conclude that they have no direct role in the construction of more complex, applications-oriented models and associated numerical tools (such as in data assimilation). Because the numerical techniques used in such models (e.g., finite-difference schemes, eddy or turbulence parameterizations) are also components of models used to simulate flows in the laboratory under similar scaling assumptions, laboratory experiments can also serve as useful "test beds" for directly evaluating and verifying the accuracy of such techniques in ways that are far more rigorous than may be possible by comparing complex model simulations solely with atmospheric or oceanic observations. Despite many advances in the formulation and development of sophisticated numerical models, there remain many phenomena (especially those involving nonlinear interactions of widely differing scales of motion) that continue to pose serious challenges to even state-of-the-art numerical models yet may be readily realizable in the laboratory. This is especially true of large-scale flow in atmospheres and oceans, for which relatively close dynamical similarity between geophysical and laboratory systems is readily achievable. Laboratory experiments in this vein therefore still have much to offer in the way of quantitative insight and inspiration to experienced researchers and fresh students alike.

1.2. ROTATING, STRATIFIED EXPERIMENTS AND GLOBAL CIRCULATION OF ATMOSPHERES AND OCEANS

At its most fundamental level, the general circulation of the atmosphere is but one example of thermal convection in response to impressed differential heating by heat sources and sinks that are displaced in both the vertical *and/or the horizontal* in a rotating fluid of low viscosity and thermal conductivity. Laboratory experiments investigating such a problem should therefore include at least these attributes and be capable of satisfying at least some of the key scaling requirements for dynamical similarity to the relevant phenomena in the atmospheric or oceanic system in question. Such experimental systems may then be regarded [e.g., *Hide*, 1970; *Read*, 1988] as schematically representing key features of the circulation in the absence of various complexities associated, for example, with radiative transfer, atmospheric chemistry, boundary layer turbulence, water vapor, and clouds in a way that is directly equivalent to many other simplified and approximated mathematical models of dynamical phenomena in atmospheres and oceans.

Experiments of this type are by no means a recent phenomenon, with examples published as long ago as the mid to late nineteenth century [e.g., *Vettin*, 1857, 1884; *Exner*, 1923]; see *Fultz* [1951] for a comprehensive review of this early work. *Vettin* [1857, 1884] had the insight to appreciate that much of the essence of the large-scale atmospheric circulation could be emulated, at least in principle, by the flow between a cold body (representing the cold, polar regions) placed at the center of a rotating, cylindrical container and a heated region (representing the warm tropics) toward the outside of the container (see Figure 1.2). Vettin's experiments used air as the convecting fluid, contained within a bell jar on a rotating platform. As one might expect of a nineteenth century gentleman, he then used cigar smoke to visualize the flow patterns, demonstrating phenomena such as convective vortices and larger scale overturning circulations. However, these experiments only really explored the regime we now know as the axisymmetric or "Hadley"

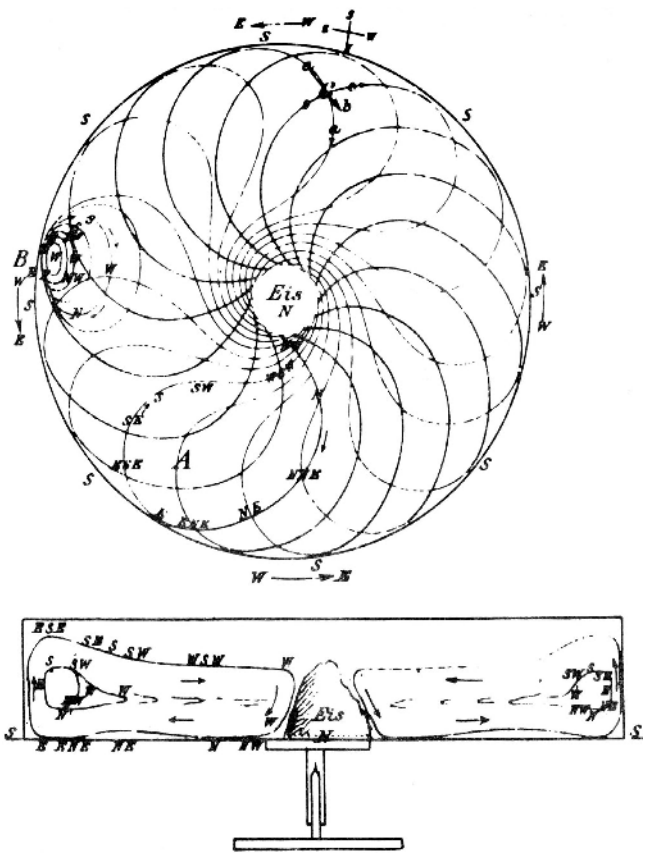

Figure 1.2. Selection of images adapted from *Vettin* [1884] (see http://www.schweizerbart.de). Reproduced with permission from the publishers, showing the layout of his rotating convection experiment and some results.

regime, since the flows Vettin observed showed little evidence for the instabilities we now know as "baroclinic instability" or "sloping convection" [*Hide and Mason*, 1975].

As an historical aside, it is interesting to note that early meteorologists such as *Abbe* [1907] intended for laboratory experiments of this type to serve also as models of the first kind, i.e., as application-oriented, predictive model atmospheres. They realized that, while it might be possible in principle to use the equations of atmospheric dynamics to determine future weather, they were beyond the capacity of mathematical analysis to solve. They hoped to use these so-called mechanical integrators [*Rossby*, 1926] under complicated external forcing corresponding to the observations of the day to reproduce and predict very specific flow phenomena observed in the atmosphere. It was anticipated that many such experiments would be built representing different regions of Earth's surface or different times of year, such as when the cross-equatorial airflow is perturbed by the monsoon [*Abbe*, 1907] (although it is not clear whether such an experiment was ever constructed). However, following the development of the electronic computer during the first half of the twentieth century and *Richardson's* [1922] pioneering work on numerical weather prediction, these more complex laboratory representations of the atmosphere were superseded.

The later experiments of *Exner* [1923] explored a different regime in which baroclinic instability seems to have been present. The flows he demonstrated were evidently quite disordered and irregular, likely due in part to the parameter regime he was working in but also perhaps because of inadequate control of the key parameters. It was not until the late 1940s, however, that Fultz began a systematic series of experiments at the University of Chicago on rotating fluids subject to horizontal differential heating in an open cylinder (hence resulting in the obsolete term "dishpan experiment") and set the subject onto a firm footing. Independently and around the same time, *Hide* [1958] began his first series of experiments at the University of Cambridge on flows in a heated rotating annulus, initially in the context of fluid motions in Earth's liquid core. By carrying out an extensive and detailed exploration of their respective parameter spaces, both of these pioneering studies effectively laid the foundations for a huge amount of subsequent work on elucidating the nature of the various circulation regimes identified by Fultz and Hide, subsequently establishing their bifurcations and routes to chaotic behavior, developing new methods of modeling the flows using numerical techniques, and measuring them using ever more sophisticated methods, especially via multiple arrays of in situ probes and optical techniques that exert minimal perturbations to the flow itself.

An important aspect of the studies by Fultz and Hide was their overall agreement in terms of robustly identifying many of the key classes of circulation regimes and locating them within a dimensionless parameter space. A notable exception to this, at least in early work, was the lack of a regular wave regime in Fultz's open cylinder experiments, in sharp contrast to the clear demonstration of such a regime in Hide's annulus. As further discussed below, this led to some initial suggestions [*Davies*, 1959] that the existence of this regime was somehow dependent on having a rigid inner cylinder bounding the flow near the rotation axis. This was subsequently shown not to be the case in open cylinder experiments by Fultz himself [*Spence and Fultz*, 1977] and by Hide and his co-workers [*Hide and Mason*, 1970; *Bastin and Read*, 1998] and two-layer [*Hart*, 1972, 1985] experiments that clearly showed that persistent, near-monochromatic baroclinic wave flows could be readily sustained in a system without a substantial inner cylinder. It is likely, therefore, that early efforts failed to observe such a regular regime in the thermally driven, open cylinder geometry because of a lack of

close experimental control, e.g., of the rotation rate or the static stability in the interior.

Earlier studies in this vein were extensively reviewed by *Hide* [1970] and *Hide and Mason* [1975]. More recently, significant advances have been presented by various groups around the world, including highly detailed experimental studies in the "classical" axisymmetric annulus of synoptic variability, vacillations, and the transitions to geostrophically turbulent motions by groups at the Florida State University [e.g., *Pfeffer et al.*, 1980; *Buzyna et al.*, 1984], the UK Met Office and Oxford University [e.g., *Read et al.*, 1992; *Früh and Read*, 1997; *Bastin and Read*, 1997, 1998; *Wordsworth et al.*, 2008], several Japanese universities [e.g., *Ukaji and Tamaki*, 1989; *Sugata and Yoden*, 1994; *Tajima et al.*, 1995, 1999; *Tamaki and Ukaji*, 2003], and, most recently, the Bremen/Cottbus group in Germany [*Sitte and Egbers*, 2000; *von Larcher and Egbers*, 2005; *Harlander et al.*, 2011] and the Budapest group in Hungary [*Jnosi et al.*, 2010]. These have been complemented by various numerical modeling studies [e.g., *Hignett et al.*, 1985; *Sugata and Yoden*, 1992; *Read et al.*, 2000; *Maubert and Randriamampianina*, 2002; *Lewis and Nagata*, 2004; *Randriamampianina et al.*, 2006; *Young and Read*, 2008; *Jacoby et al.*, 2011]. In addition, the range of phenomena studied in the context of annulus experiments have been extended through modifications to the annulus configuration to emulate the effects of planetary curvature (i.e., a β-effect) [e.g., *Mason*, 1975; *Bastin and Read*, 1997, 1998; *Tamaki and Ukaji*, 2003; *Wordsworth et al.*, 2008; *von Larcher et al.*, 2013] and zonally asymmetric topography [e.g., *Leach*, 1981; *Li et al.*, 1986; *Bernadet et al.*, 1990; *Read and Risch*, 2011]; see also Chapters 2, 3, 7, 16, and 17 in this volume.

The existence of regular, periodic, quasi-periodic, or chaotic regimes in an open cylinder was also a major feature of another related class of rotating, stratified flow experiments using discrete two-layer stratification and mechanically-imposed shears. *Hart* [1972] introduced this experimental configuration in the early 1970s, inspired by the theoretical work of *Phillips* [1954] and *Pedlosky* [1970, 1971] on linear and weakly nonlinear instabilities of such a two-layer, rotating flow system. Because of its simpler mode of forcing and absence of complicated boundary layer circulations, these kinds of two-layer systesm were more straightforward to analyze theoretically, allowing a more direct verification of theoretical predictions in the laboratory than has typically proved the case with the thermally driven systems. Subsequent studies by Hart [*Hart*, 1979, 1980, 1985, 1986; *Ohlsen and Hart*, 1989a,1989b] and others [e.g., *King*, 1979; *Appleby*, 1982; *Lovegrove et al.*, 2000; *Williams et al.*, 2005, 2008] have extensively explored this system, identifying various forms of vacillation and low-dimensional chaotic behaviors as well as the excitation of small-scale, interfacial inertia-gravity waves through interactions with the quasi-geostrophic baroclinic waves.

In this chapter, we focus on the "classical" thermally driven, rotating annulus system. In Section 1.3 we review the current state of understanding of the rich and diverse range of flow regimes that may be exhibited in thermal annulus experiments from the viewpoint of experimental observation, numerical simulation, and fundamental (mainly quasi-geostrophic) theory. This will include the interpretation of various empirical experimental observations in relation to both linear and weakly nonlinear baroclinic instability theory. One of the key attributes of baroclinic instability and "sloping convection" is its role in the transfer of heat within a baroclinic flow. In Section 1.4 we examine in some detail how heat is transported within the baroclinic annulus across the full range of control parameters, associated with both the boundary layer circulation and baroclinically unstable eddies. This leads naturally to a consideration of how axisymmetric boundary layer transport and baroclinic eddy transports scale with key parameters and hence how to parameterize these transport processes, both diagnostically and prognostically, in a numerical model for direct comparison with recent practice in the ocean modeling community. Finally, in Section 1.5 we consider the overall role of annulus experiments in the laboratory in continuing to advance understanding of the global circulation of planetary atmospheres and oceans, reviewing the current state of research on delineating circulation regimes obtained in large-scale circulation models in direct comparison with the sequences of flow regimes and transitions in the laboratory. The results strongly support many parallels between laboratory systems and planetary atmospheres, at least in simplified models, suggesting a continuing important role for the former in providing insights for the latter.

1.3. FLOW REGIMES AND TRANSITIONS

The typical construction of the annulus is illustrated schematically in Figure 1.1 and consists of a working fluid (usually a viscous liquid, such as water or silicone oil, though this can also include air [e.g., see *Maubert and Randriamampianina*, 2002; *Randriamampianina et al.*, 2006; *Castrejón-Pita and Read*, 2007] or other fluids, including liquid metals such as mercury [*Fein and Pfeffer*, 1976]) contained in the annular gap between two coaxial circular, thermally conducting cylinders, that can be rotated about their common (vertical) axis. The cylindrical sidewalls are maintained at constant but different temperatures, with a (usually horizontal) thermally insulating lower boundary and an upper boundary that is also thermally insulating and either rigid or free (i.e., without a lid).

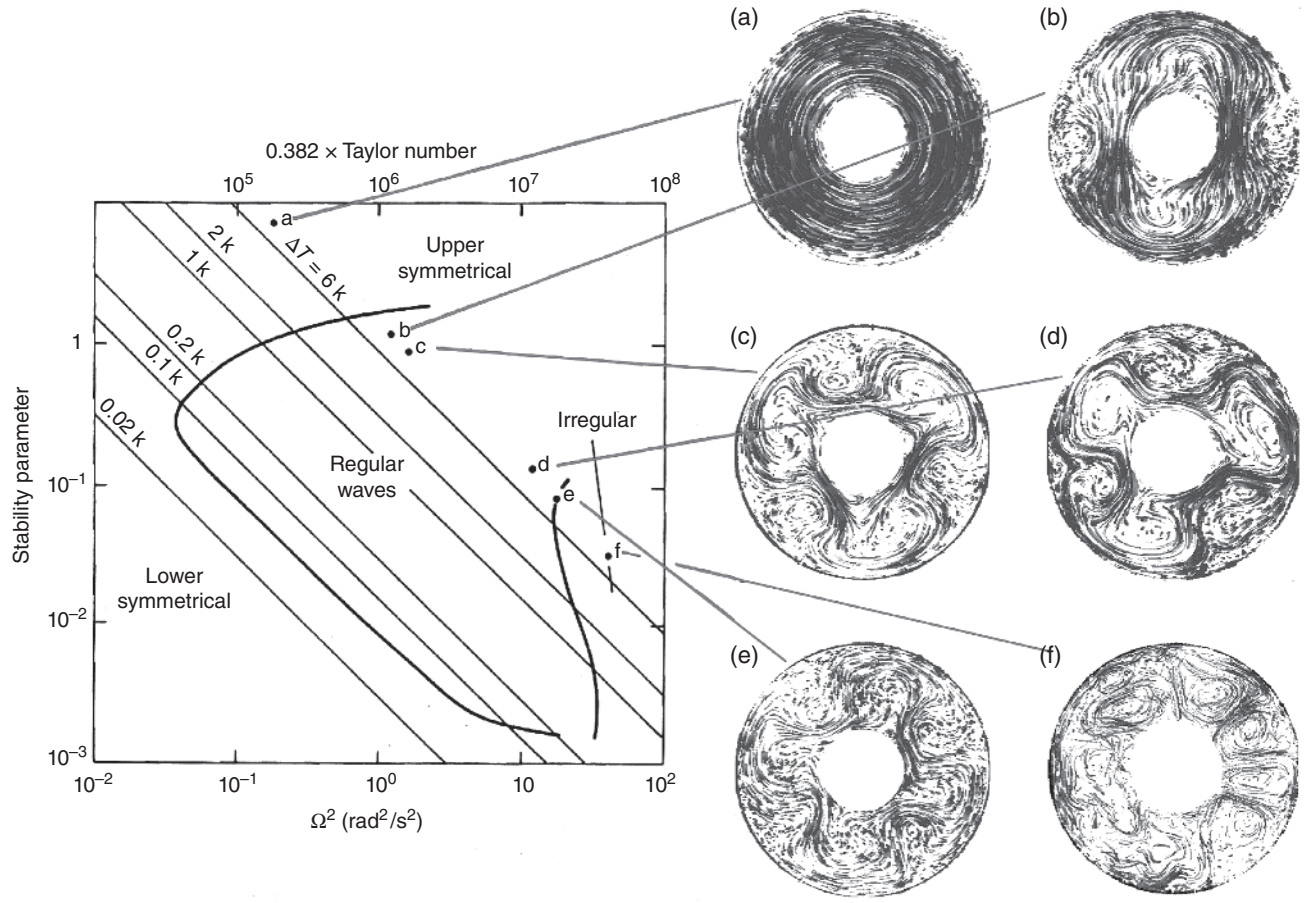

Figure 1.3. Schematic regime diagram for the thermally driven rotating annulus in relation to the thermal Rossby number Θ (or stability parameter, $\propto \Omega^{-2}$) and Taylor number $\mathcal{T} \propto \Omega^2$, showing some typical horizontal flow patterns at the top surface, visualized as streak images at upper levels of the experiment.

1.3.1. Principal Flow Regimes

Although a number of variations in these boundary conditions have been investigated experimentally, almost all such experiments are found to exhibit the same three or four principal flow regimes, as parameters such as the rotation rate Ω or temperature contrast ΔT are varied. These consist of (I) axisymmetric flow (in some respects analogous to Hadley flow in Earth's tropics and frequently referred to as the "upper-symmetric regime"; see below) at very low Ω for a given ΔT (that is not too small); (II) regular waves at moderate Ω; and (III) highly irregular, aperiodic flow at the highest values of Ω attainable. In addition, (IV) axisymmetric flows occur at all values of Ω at a sufficiently low temperature difference ΔT (a diffusively dominated regime termed "lower symmetric" [*Hide and Mason*, 1975, *Ghil and Childress*, 1987] to distinguish it from the physically distinct "upper-symmetric" mentioned above). The location of these regimes are usually plotted on a "regime diagram" with respect to the two (or three) most significant dimensionless parameters. These are typically

(a) a stability parameter or "thermal Rossby number"

$$\Theta = \frac{g\alpha \Delta T d}{[\Omega (b-a)]^2}, \tag{1.1}$$

providing a measure of the strength of buoyancy forces relative to Coriolis accelerations;

(b) a Taylor number

$$\mathcal{T} = \frac{\Omega^2 (b-a)^5}{\nu^2 d}, \tag{1.2}$$

measuring the strength of Coriolis accelerations relative to viscous dissipation; and

(c) the Prandtl number

$$\mathrm{Pr} = \frac{\nu}{\kappa}. \tag{1.3}$$

Here g is the acceleration due to gravity, α the thermal expansion coefficient of the fluid, ν the kinematic viscosity, κ the thermal diffusivity, and a, b, and d the radii of

the inner and outer cylinder and the depth of the annulus, respectively. Figure 1.3 shows a schematic form of this diagram with the locations of the main regimes indicated.

From a consideration of the conditions under which waves occur in the annulus (especially the location in the parameter space of the upper-symmetric transition) and a comparison with the results of linear instability theory, it is clear that the waves in the annulus are fully developed manifestations of baroclinic instability (often referred to as "sloping convection" from the geometry of typical fluid trajectories; for example, see *Hide and Mason* [1975]). Since these flows occur in the interior of the annulus (i.e., outside ageostrophic boundary layers) under conditions appropriate to quasi-geostrophic scaling, a dynamical similarity to the large-scale midlatitude cyclones in Earth's atmosphere is readily apparent, though with rather different boundary conditions. A more detailed discussion of the properties of these flows is given below and by *Hide and Mason* [1975] and *Ghil and Childress* [1987]. Associated with this conclusion is the implication that the waves develop in order to assist in the transfer of heat both upward (enhancing the static stability) and horizontally down the impressed thermal gradient (i.e., tending to reduce the impressed horizontal gradient). The action of heat transport by the waves and axisymmetric flows will be considered in the next section.

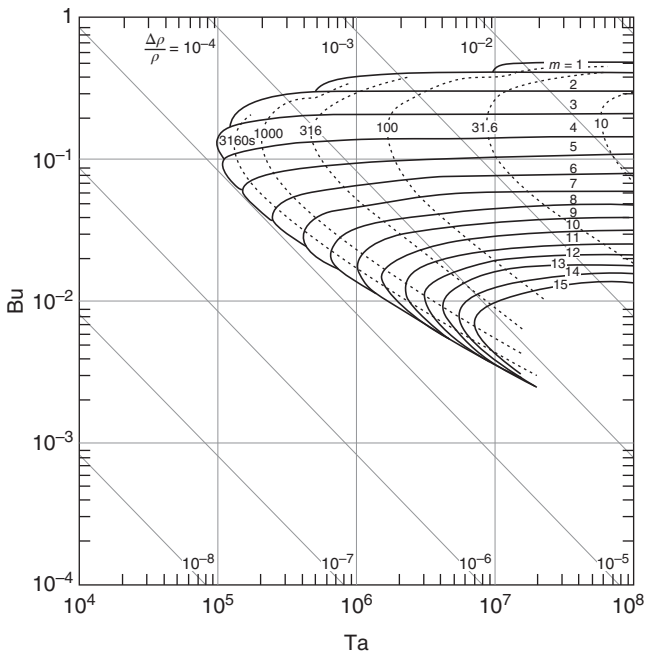

Figure 1.4. Regime diagram based on the extension of Eady's baroclinic instability theory to include Ekman layers and flat, horizontal boundaries. The wave number of maximum instability is indicated by integer numbers and the transition curves and contours of e-folding time are given on a Burger number (Bu $\sim \Theta$; see *Hide and Mason* [1975]) against $\mathcal{T}$ plot. (Adapted from *Mason* [1975] by permission of the Royal Society).

1.3.2. Axisymmetric/Wave Transition and Linear Instability Theory

The previous section indicated the conditions under which baroclinic waves occur in the annulus and their role as a means of transferring heat upward and against the horizontal temperature gradient. The Eady model of baroclinic instability has been commonly invoked as an idealized, linearized conceptual model to account for the onset of waves from axisymmetric flow [*Hide*, 1970; *Hide and Mason*, 1975, *Ghil and Childress*, 1987]. Although the Eady model is highly idealized, it does seem to predict the location of the onset of large-amplitude waves remarkably close to the conditions actually observed, at least at high Taylor number (note that the Eady problem in its "classical form" is inviscid). Apparent agreement can be made even closer if the Eady problem is modified to include Ekman boundary layers by replacing the $w = 0$ boundary condition with the Ekman compatibility condition

$$w = \frac{\mathcal{E}^{1/2}}{\sqrt{2}\mathrm{Ro}}\nabla^2\psi, \qquad z = 0, 1, \tag{1.4}$$

where ψ is the stream function for the horizontal flow. This naturally brings in the Taylor number familiar to experimentalists (via Ekman number $\mathcal{E}$) and leads to a plausibly realistic envelope of instability at low Taylor number (see Figure 1.4), supporting the hypothesis [*Hide and Mason*, 1975] that the "lower symmetric transition" is frictionally dominated.

The structure of the most rapidly growing instability has certain characteristic features in terms of, for example, phase tilts with height. In the thermal annulus, steady baroclinic waves are also seen to exhibit many of these features, as determined from experiment and numerical simulation. The extent to which Eady theory actually provides a complete theoretical description of the instability problem in annulus experiments, however, is a somewhat more complicated question than it at first appears. The dominant instability in the Eady model relies on the existence of horizontal temperature gradients on horizontal boundaries for the required change of sign in the lateral gradient of quasi-geostrophic potential vorticity, $\partial\overline{q}/\partial y$, for instability [e.g., *Charney and Stern*, 1962]. Elsewhere, the flow is constructed such that $\partial\overline{q}/\partial y = 0$. In practice, however, strong horizontal mass transports in the Ekman layers result in almost no horizontal temperature gradients at the boundaries; in reality $\partial\overline{q}/\partial y$ changes sign smoothly in the interior (e.g., see Figure 1.17c later). Thus, instability of an internal baroclinic jet is arguably a more appropriate starting point, preferably including a

consideration of lateral shears. This was considered by *Bell and White* [1988], who examined the stability of an idealized internal zonal jet flow in a straight, rectangular channel of the form

$$U = \frac{1}{2}(1 - a_s + a_s - \sin \pi y) \sin \pi z, \qquad (1.5)$$

where a_s is a constant that determines the degree of horizontal barotropic shear in the otherwise baroclinic jet. If full account is taken of lateral shear in such an internal jet (by varying a_s), however, the critical Burger number for the onset of waves is found to vary by a factor of $O(10)$. The precisely applicable value is likely dependent upon subtle details of the shape of the zonal flow and the imposed lateral boundary conditions, since the true boundary conditions at the sides of the geostrophic interior ought really to take proper account of the complex viscous boundary layer structures (e.g., Stewartson layers), although impermeable, free-slip boundaries have typically been employed (for mathematical convenience) in most theoretical studies to date.

Recent exceptions to this include the two-layer studies by *Mundt et al.* [1995a, 1995b] and the analysis of the full thermal annulus problem by *Lewis and Nagata* [2004]. *Mundt et al.* [1995a] examined the linear (and nonlinear) stability of a quasi-geostrophic, two-layer jet in a rectilinear channel in which internal viscosity was included in deriving the zonally symmetric basic state. This led to the formation of viscous (Stewartson) boundary layers adjacent to the sidewalls of the channel, within which strong zonal shear developed as the flow adjusted to the nonslip condition at each boundary. This was then shown to modify the critical Froude number for instability by a factor $O(1)$ for the gravest modes. Similar results were obtained by *Mundt et al.* [1995b] in cylindrical geometry, for which improved agreement with experimental measurements was shown compared with stability calculations assuming a free-slip outer boundary. The most sophisticated approach applied so far for the thermal annulus configuration was by *Lewis and Nagata* [2004], who used numerical continuation techniques to solve for the linear stability boundary (as a function of Θ and $\mathcal{T}$) of an axisymmetric baroclinic zonal jet in cylindrical geometry using the full Navier-Stokes equations for a viscous, Boussinesq fluid. The results indicated good agreement with the location of both the upper and lower symmetric transitions as found in laboratory experiments. They also indicated the influence of centrifugal buoyancy in modifying the stability boundary at the lower symmetric transition. These calculations all serve to demonstrate the quantitative success of linear stability theory in accounting quantitatively for the onset of the principal mode of baroclinic instability in both two-layer and continuously stratified rotating tank experiments as a supercritical global bifurcation.

1.3.3. Steady Waves and Equilibration: Weakly Nonlinear Theory

As waves grow in strength from an initial zonal flow, they typically equilibrate to either a steady or periodically varying amplitude ("amplitude vacillation")or even to a weakly chaotic flow. The linear models of baroclinic instability cannot account for equilibration and vacillation, and so we must consider the effects of nonlinearity in the interaction between the growing wave and the basic zonal flow. Weakly nonlinear theory was developed in the late 1960s as a means of introducing nonlinearity into linear instability problems while keeping the mathematics analytically tractable. The basic assumption of this approach is that the flow in which the wave grows is only weakly supercritical, and so only a small range of wave numbers is unstable and grows relatively slowly. More detailed discussions can be found [e.g., *Drazin*, 1978; *Hocking*, 1978; *Ghil and Childress*, 1987; *Pedlosky*, 1987].

Consider a zonal flow under conditions just inside the stability threshold with weak supercriticality Δ. Because the stability boundary is then asymptotically quadratic in zonal wave number k about the wave number of the first mode to go unstable k_c (see Figure 1.5), a small range of $k \sim \Delta^{1/2}$ is destabilized. In a periodic x domain where k is discretized, this may permit only one unstable wave number. We introduce a "slow" time scale τ defined by

$$\tau = \Delta^{1/2} t, \qquad \Delta \ll 1, \qquad (1.6)$$

(in the sense that it advances more slowly than "normal time" t) and solve for normal modes of the following wavelike form in the zonal (x) direction:

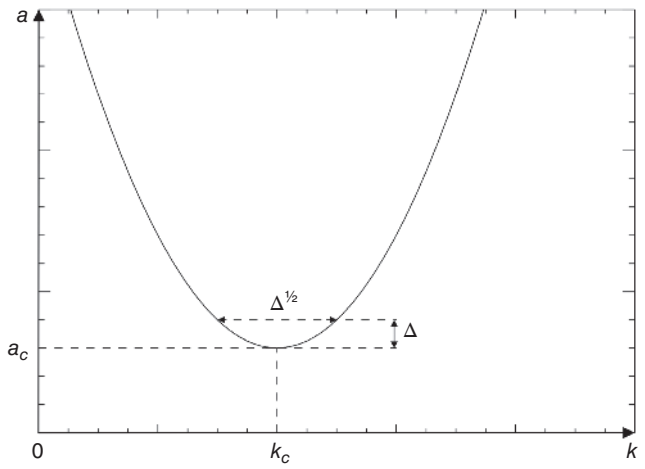

Figure 1.5. Schematic stability diagram showing the assumed (quadratic) form of the critical curve $a(k)$ as a function of wave number k in the vicinity of the first unstable mode with wave number k_C.

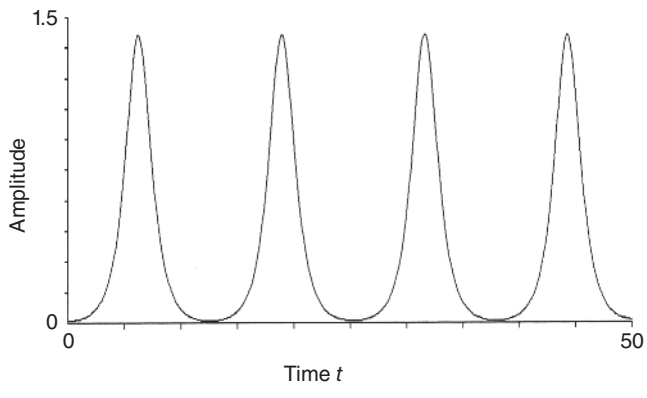

Figure 1.6. A typical solution to equations (1.9) and (1.10) showing sustained amplitude oscillations.

$$\tau = \mathcal{R}\{A(\tau)F(y,z)\exp k(x-ct)\}, \tag{1.7}$$

where y is the meridional coordinate and z is in the vertical in the presence of a zonal flow of the form

$$U = U(y,z) + V(\tau)G(y,z). \tag{1.8}$$

Here A and V are respectively the slowly varying amplitudes of the wave and the correction to the zonal flow due to the nonlinear self-interaction of the wave, whose spatial structure is represented by $Gy,z)$. The resulting evolution equations for A and V depend upon the relative magnitude of viscous dissipation:

(i) Weak Dissipation ($\mathcal{E}^{1/2}/\mathrm{Ro} \ll O(\Delta^{1/2})$)

Examples include the Eady or two-layer Phillips problems with no Ekman layers [e.g., *Pedlosky*, 1987]. It can be shown that the problem then reduces to coupled ordinary differential equations (ODEs) of the form

$$\frac{d^2A}{d\tau^2} = a_1A - |a_3|A^3, \tag{1.9}$$

$$\frac{dV}{d\tau} = a_4\frac{dA}{d\tau}, \tag{1.10}$$

typically resulting in a sustained amplitude modulation, or "vacillation," associated with the exchange of potential energy between wave and zonal flow (e.g., see Figure 1.6).

(ii) Stronger Dissipation ($\mathcal{E}^{1/2}/\mathrm{Ro} = O(1)$)

Examples include the Eady and Phillips problems with Ekman damping. It can be shown that the amplitude equations reduce to the well-known Landau equation [e.g., see *Pedlosky*, 1971; *Romea*, 1977; *Drazin*, 1978; *Hocking*, 1978]

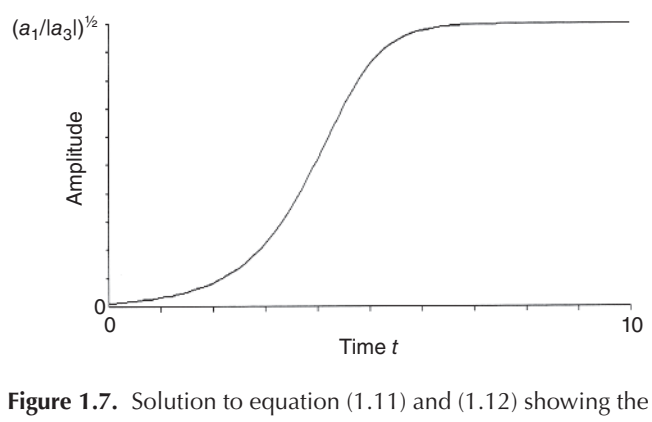

Figure 1.7. Solution to equation (1.11) and (1.12) showing the approach to a steady equilibrium.

$$\frac{dA}{d\tau} = a_1A - |a_3|A^3, \tag{1.11}$$

$$V = a_4|A|^2, \tag{1.12}$$

resulting typically in an asymptotic equilibration toward a steady amplitude $A = (a_1/|a_3|)^{1/2}$ (see Figure 1.7).

These models, of course, represent a considerable oversimplification of the real equilibration processes in fully developed baroclinic instability. Indeed, *Boville* [1981] noted that *Pedlosky*'s [1970] approach led to significant inaccuracies in predicting the amplitude behavior of baroclinic waves and failed to observe the predicted amplitude oscillations close to minimum critical shear. Subsequent work [*Pedlosky*, 1982a, 1982b; *Warn and Gauthier*, 1989; *Esler and Willcocks*, 2012] suggests that the dynamical equilibration is more typically dominated by the behavior of a nonlinear critical layer that develops within the flow, leading to the wrapping up and eventual homogenization of potential vorticity. The equilibrated state may then result in convergence toward a steady wave state via a series of damped amplitude oscillations. The analytical solutions of *Warn and Gauthier* [1989] even produced periodic amplitude oscillations under certain conditions, resembling an amplitude vacillation, but in which potential vorticity is reversibly mixed and unmixed. This is only strictly applicable under conditions of weak friction close to marginal instability. The recent work of *Willcocks and Esler* [2012] also suggests that the mode of equilibration via a Landau equation, predicted in the models of *Pedlosky* [1971] and *Romea* [1977], probably applies mainly to the dissipatively destabilized instability that occurs for shears less than the critical shear in the inviscid problem in the presence of Ekman friction [*Holopainen*, 1961; *Boville*, 1981]. The full applicability of any of these models, however, still remains to be verified in detail in laboratory experiments or fully nonlinear numerical simulations in continuously stratified flows.

1.3.4. Wave Number Selection

Within the regular baroclinic wave regime, the flow tends to equilibrate typically (in the absence of a strong β-effect, e.g., associated with topographically sloping boundaries) to a state dominated by a single azimuthal wave number and its harmonics, which may be steady, quasi-periodic, or chaotic. The mechanisms by which rotating annulus waves select which wave number to favor at fully nonlinear equilibration are still not fully understood but seem likely to share some aspects in common with mechanisms identified in simple, weakly nonlinear, spectrallytruncated models of baroclinic instability. Such models [e.g., see above and *Pedlosky*, 1970; *Drazin*, 1970; *Pedlosky*, 1971] represent only the leading order nonlinear interactions between a single mixed baroclinic-barotropic traveling wave and the background ($m = 0$) zonal flow (i.e., suppressing quadratic and higher order wave-wave interactions). The nonlinear self-interaction of a growing, linearly unstable wave generates a correction to the $m = 0$ zonal flow (at second order in wave amplitude) that feeds back on the growth rate, eventually reducing it to zero (a steady wave state, for which the modal amplitude equations may asymptotically reduce to a set of Landau equations in the presence of some frictional damping), or with a more complicated, quasi-periodic or chaotic time dependence [e.g., see *Lovegrove et al.*, 2001, 2002], for which the modal amplitude equations may reduce asymptotically to the classical real or complex Lorenz equations.

When more than one distinct wave number mode is able to grow from infinitesimal amplitude on a given zonal flow, weakly nonlinear models do not provide a unique answer as to what mechanism will act to select the dominant mode. However, one commonly found factor is for the flow to preferentially select the mode that is capable of releasing the most available potential energy (APE) from the initial flow [*Hart*, 1981]. In practice, this may correspond to the mode that can reach the largest barotropic amplitude [*Hart*, 1981; *Appleby*, 1988] provided nonlinear wave-wave interactions are absent. Where wave-wave interactions are permitted, the mode selection may become hysteretic such that a nonoptimal wave mode (i.e., one that does not release the maximum possible APE) may persist as the dominant mode if it was previously dominant under more favorable conditions at an earlier time. This is found to manifest itself within the regular flow regime as intransitivity (i.e., multiple equilibrium states), in which two or more alternative flows with differing azimuthal wave number m can occur for a given set of parameters [e.g., *Hide*, 1970; *Hide and Mason*, 1975]. The state obtained in any particular experiment implicitly depends upon the initial conditions. In addition, transitions between different states in the regular regime, achieved by slowly changing the external parameters, often exhibit hysteresis [e.g., *Hide and Mason*, 1975; *Sitte and Egbers*, 2000; *von Larcher and Egbers*, 2005] in that the location of a transition in parameter space depends upon the direction from which that transition is approached (e.g., transitions from $m = 3 \rightarrow 4$ do not occur at the same point as $m = 4 \rightarrow 3$). In a situation where the forcing that maintains the background zonal state is varied cyclically with time over a range that crosses the boundary between two or more optimal modes, this can lead to complex and chaotic behavior as the flow pattern flips erratically from one dominant mode to another [e.g., see *Buzyna et al.*, 1978].

Another issue is how an initially dominant wave flow may retain its dominance and remain indefinitely stable? The presence of wave-wave and higher order nonlinear interactions might be expected to permit the possibility of secondary instabilities of the primary dominant wave mode, at least in principle, thereby preventing the sustained dominance of a single baroclinic wave mode. *Hide* [1958] and *Hide and Mason* [1975] showed empirical evidence from a range of early experiments that, depending upon the radius ratio between inner and outer cylinders, there was a maximum azimuthal wave number of a stable and persistent dominant wave such that its azimuthal wavelength always seemed to exceed roughly 1.5 times the radial extent of the wave, i.e.,

$$m_{\max} \gtrsim \frac{2\pi(b+a)}{3(b-a)}. \tag{1.13}$$

The prototypical idealized model for such a situation considers the stability of the basic Rossby-Haurwitz (RH) mode on the sphere to wavelike barotropic perturbations [*Lorenz*, 1972; *Hoskins*, 1973; *Baines*, 1976], although this has also been generalized to investigate baroclinic perturbations and instabilities of the basic RH wave [e.g., see *Kim*, 1978; *Grotjahn*, 1984a, 1984b]. The principal criterion for barotropic stability of the RH wave can be interpreted in relation to Fjørtoft's theorem for energy transfer in a quasi-geostrophic flow [*Fjørtoft*, 1953], for which both energy and squared vorticity must be conserved in non dissipative nonlinear interactions. This essentially requires that a given wave mode must lose energy simultaneously to both a higher *and a lower* wave number mode. Thus, the longest wave number modes capable of fitting into the domain tend to be relatively stable because of the unavailability of longer wavelength modes to which they can lose energy in an instability. Such an interpretation appears to be consistent with the criterion in equation (1.13) found by *Hide* [1958] and *Hide and Mason* [1975] for the maximum azimuthal wave number that can sustain a persistent dominant wave flow.

Recent work by *Young and Read* [2013] suggests that barotropic instability may not be the only possible mechanism for breakdown of regular baroclinic wave flows.

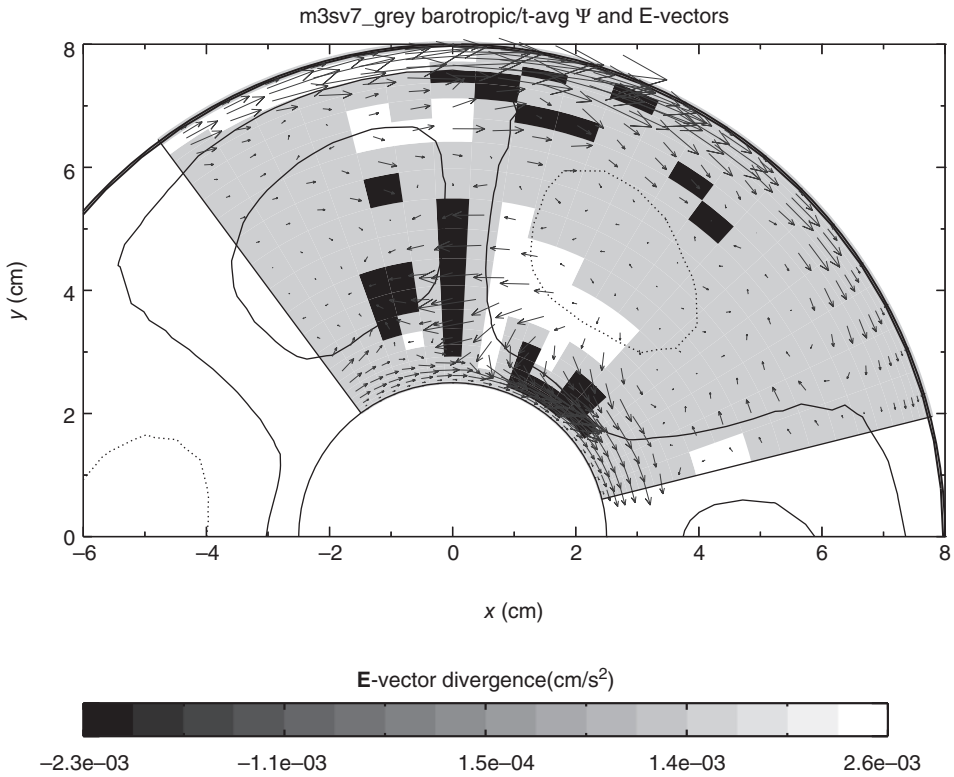

Figure 1.8. **E**vectors for chaotic flow in the annulus. The black contour lines show the assimilated barotropic time-averaged horizontal stream function (contours below the middle of the range are dotted), and the grey vectors are the barotropic time-averaged **E** vectors. The shading shows the **E**-vector divergence: black is up to -5×10^{-4} cm/s^2, grey is between -5×10^{-4} cm/s^{-2} and $+5 \times 10^{-4}$ cm/s^2, and white is above $+5 \times 10^{-4}$ cm/s^2. The flow is at $\Omega = 3.1$ rad/s with $T_b - T_a \approx 4.02$°C. (Adapted from *Young and Read* [2013] with permission of John Wiley & Sons, Inc.)

Based on sequences of laboratory measurements assimilated into a Boussinesq Navier-Stokes numerical model of the annulus, *Young and Read* [2013] found that localized, small-scale eddies shed from the cyclonic troughs of a large-scale baroclinic wave mode may be consistent with a localized baroclinic instability. Figure 1.8 shows the **E**vectors [*Hoskins et al.*, 1983; *James*, 1994] for these measurements at the highest rotation rate investigated. The barotropic **E**vector is a horizontal vector defined from correlations between the $x-y$ components of the horizontal velocity (u, v) by

$$\mathbf{E} = (E_x, E_y) = (\overline{v'^2} - \overline{u'^2}, -\overline{u'v'}), \tag{1.14}$$

where the overbar represents a timeaverage and primed quantities are deviations from the time-mean flow. Its divergence provides a measure of the interaction between the time-mean flow and transient eddies such that $\nabla \cdot \mathbf{E} > 0$ implies a tendency for eddies to strengthen the mean flow [*Hoskins et al.*, 1983]. For **E**vectors pointing in the positive azimuthal direction, there is anticyclonic cyclogenesis between the divergent region and the outer cylinder, cyclonic cyclogenesis between the convergent region and the outer cylinder, and vice versa toward the inner cylinder. For the baroclinic annulus flows considered, *Young and Read* [2013] found the **E**vectors became more strongly convergent/divergent as the rotation rate increased. This acted to reinforce the main cyclone but weaken the part extending into the anticyclonic region, associated with the shedding of small-scale vortices, and doing so more and more as the rotation rate increased. The main baroclinic wave was found to be barotropically stable according to *Bell*'s [1989] criterion, but the instability was consistent with *Kim*'s [1989] observation that baroclinic Rossby waves may be baroclinically unstable if the internal Rossby deformation radius L_D is much smaller than a characteristic horizontal length scale L representative of the large-scale wave, in this case comparable with the annular gap width $b - a$. In this flow $L \gg L_D$ with increasing supercriticality (smaller values of Θ) as the rotation rate increased (as $L_D \propto 1/\Omega$), consistent with an interpretation of the chaotic vortex-shedding phenomenon discussed above as a secondary baroclinic instability of the large-scale wave.

1.3.5. Vacillating Waves and Wave-Zonal Flow Interactions

Baroclinic waves in the regular wave regime may be either steady (apart from a slow drift) or "vacillating" (i.e., with a periodic or nearly periodic time dependence; see Chapter 3 for a more detailed discussion). Laboratory observations of "amplitude vacillation" indicate that (for fluids with Pr $\gg$ 1) it occurs close to the upper stability threshold of its wave number m, around where a transition from m to $m-1$ is observed, at moderate-high Taylor number. At lower values of Pr, however, it appears that this transition sequence is reversed, with transitions, for example using air as the working fluid (with Pr $\simeq$ 0.7), from steady waves into the vacillating regime as $\mathcal{T}$ is *increased* [e.g., *Randriamampianina et al.*, 2006; *Castrejón-Pita and Read*, 2007]; see also Chapter 16 in this volume. The "vacillating" state then comprises the periodic modulation of both the amplitude and drift frequency of the wave on a time scale $\sim$ 10 – 100 "days". Figure 1.9 shows a sequence of streak images taken from a typical m = 3 flow undergoing an amplitude vacillation cycle at a level around 0.8d above the annulus base. This clearly shows the wave amplitude growing, reaching a maximum in amplitude in Figure 1.9d and then decaying before the cycle repeats. The wave is modulated in both amplitude and drift rate (phase speed) during the cycle, indicating a nonlinear interaction with the background zonal flow.

More detailed diagnostics show periodic variations in total heat transport and in potential energy exchanges between the wave and zonal flow [see *Pfeffer et al.*, 1980; *Hignett et al.*, 1985]. In particular variations in the slope of the azimuthal mean isotherms (see Figure 1.10) clearly show modulations in the potential energy stored in the azimuthal mean flow. The zonal flow structure (see Figure 1.10a and 1.10b) is seen to oscillate between a single jet pair at minimum wave amplitude and two double jets at maximum amplitude.

In this regard, it appears that nonlinear interactions between the dominant wave and the azimuthal mean flow are critically important for the phenomenon of amplitude vacillation. In practice, however, it may not be easy to distinguish this behavior from interference arising from a quasi-linear superposition of two wave components with the same azimuthal wave number and differing vertical structure and drift frequencies ω_1 and ω_2. Apparent "vacillation" then takes place at the difference frequency of the two components $|\omega_1 - \omega_2|$. If the two components cross-interact with the zonal flow, effects such as phase locking and zonal flow modulation may occur, reproducing several aspects of the observed flows. Some observers claim to have identified this mechanism in measurements in the laboratory [*Lindzen et al.*, 1982], though the more general relevance of this mechanism remains controversial. However, other forms of nonlinear interference vacillation, for example, involving the superposition of two modes with differing (but adjacent) azimuthal wave numbers but similar radial and vertical structures [*Ohlsen and Hart*, 1989b], may also manifest themselves as periodic modulations of baroclinic eddy variance while also modulating the azimuthal mean flow through nonlinear triad interactions of harmonics with the mean zonal flow.

Although the basic amplitude vacillation (AV) regime is typically a quasi-periodic flow characterized by two independent frequencies associated with (a) the azimuthal drift of a monochromatic wave number pattern and (b) its periodic modulation in amplitude, transitions to more chaotic states have also been observed, still apparently within the "regular" wave regime. These include transition sequences via period-doubling bifurcations to chaotic amplitude vacillations [*Hart*, 1985, 1986] and routes involving more complex transitions directly to chaos from doubly periodic "modulated" amplitude vacillation [*Farmer et al.*, 1982; *Read et al.*, 1992; *Früh and Read*, 1997]. The resulting flows were apparently consistent with the interaction of a relatively small number of spatial modes but differed in their basic azimuthal symmetry properties. Period doubling was observed as a typical route to chaos in the two-layer, open cylinder experiments of *Hart* [1985] and *Ohlsen and Hart* [1989a]. This does not seem to be typical for thermal annulus experiments, however, which tend to be dominated by higher wave number baroclinic modes ($m \gtrsim 3$). In the latter, the more typical route involves the development of a third period through the emergence of an additional wave mode that is not harmonically related to the initial dominant wave [*Read et al.*, 1992; *Früh and Read*, 1997].

However, *Young and Read* [2008] did observe a sequence of period doublings from a wave number m = 2AV flow in a set of numerical simulations which led to chaotic states consistent with the endpoint of a period-doubling cascade over limited regions of parameter space. Figure 1.11 shows two examples of such flows, illustrating chaotic ((a), (b)) and period 3 ((c), (d)) vacillations. In this regime, the amplitude modulations vary in strength, alternating between two intensities in the period 2 state with successive doublings as $\mathcal{T}$ was increased until chaotic vacillation ensued. The whole sequence shows a sequence of bifurcations as successive period doublings lead to chaotic behavior followed by an indication of period 3 "periodic windows". Figure 1.12 illustrates such a sequence at even higher values of $\mathcal{T}$ showing the maximum and minimum wave amplitudes of the equilibrated baroclinic flow at various values of $\mathcal{T}$ while keeping Θ at a fixed value of $\Theta \simeq 1.75$. This shows clear evidence of a series of period-doubling transitions with chaotic regions near points A, B, and D interspersed with regions characterized by quasi-periodic vacillations.

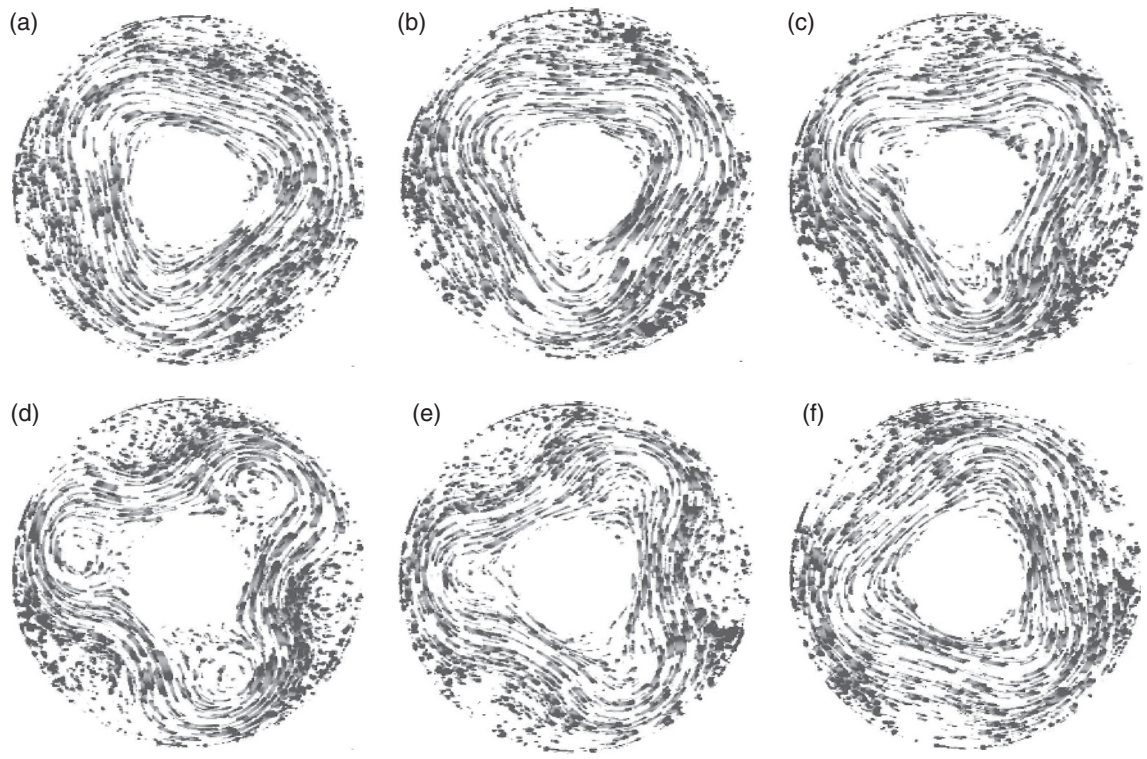

Figure 1.9. Typical horizontal flow fields (streak photographs) during an "amplitude vacillation" cycle of the rotating annulus in the same system as in Figures 1.8–1.13. For color detail, please see color plate section.

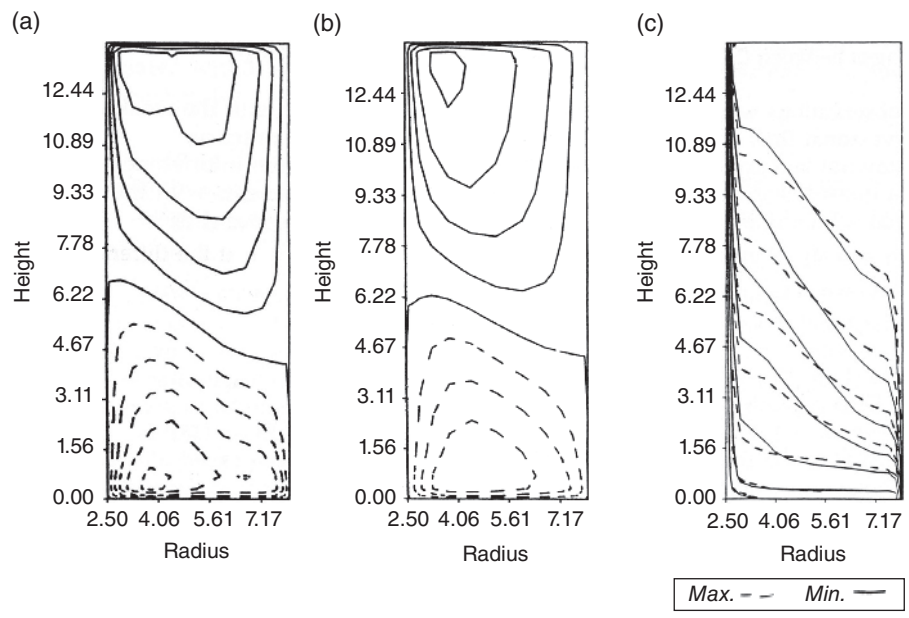

Figure 1.10. Results from numerical simulations of a baroclinic amplitude vacillation in a rotating annulus similar to that of *Hignett et al*. [1985] showing (a) azimuthal mean azimuthal flow at maximum wave amplitude, (b) azimuthal mean azimuthal flow at minimum wave amplitude, and (c) azimuthal mean temperature fields at minimum (solid) and maximum (dashed) wave amplitude during the vacillation cycle.

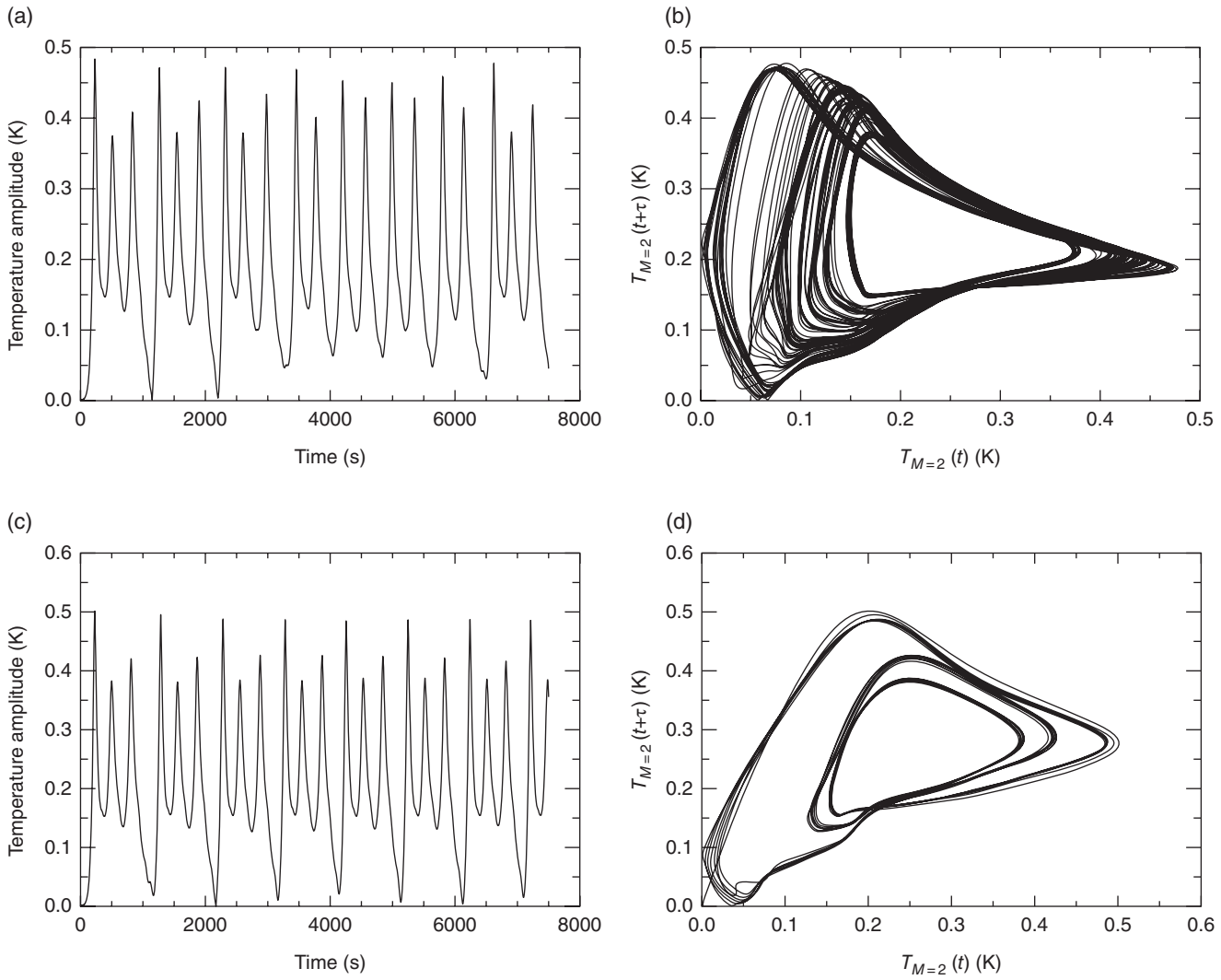

Figure 1.11. Temperature $m = 2$ amplitude time series [(a) and (c)] and delay coordinate reconstructions [(b) and (d)] in the $m = 2$AV-d period-doubled amplitude vacillation regime, obtained by *Young and Read* [2008] in Boussinesq Navier-Stokes simulations of rotating annulus flows. $\tau = 100$ s in (b) and $\tau = 85$ s in (d). Adapted from *Young and Read* [2008]. Copyright 2008, with permission from Elsevier.

Such a sequence is strongly reminiscent of the period-doubling route to chaos found in the two-layer experiments of *Hart* [1985, 1986], who showed sequences of period doublings from an $m = 1$AV flow at fixed Froude number. This would therefore appear to be a generic route to chaos in baroclinic wave flows at low enough wave numbers that sideband instabilities do not dominate the dynamics, and the main nonlinear interaction is between a single wave and the zonal flow.

This kind of bifurcation sequence has also been obtained in various studies invoking weakly nonlinear baroclinic instability theory, such as by *Pedlosky and Frenzen* [1980] for the two-layer model [see *Klein*, 1990, for a review] and *Weng et al.* [1986] for the continuously stratified Eady problem. These and other studies [e.g, see *Ghil and Childress*, 1987] have shown that the endpoint of such period-doubling sequences, even in very simple models representing the interactions of single mixed baroclinic-barotropic waves with a zonal flow, can be chaotic states of low dimension. In certain limits, several workers have shown that the single wave/zonal flow equilibration problem may reduce to a set of three coupled ODEs:

$$\frac{dX}{d\tau} = \sigma(Y - X), \tag{1.15}$$

$$\frac{dY}{d\tau} = XZ + r_a X - Y, \tag{1.16}$$

$$\frac{dZ}{d\tau} = XY - bZ, \tag{1.17}$$

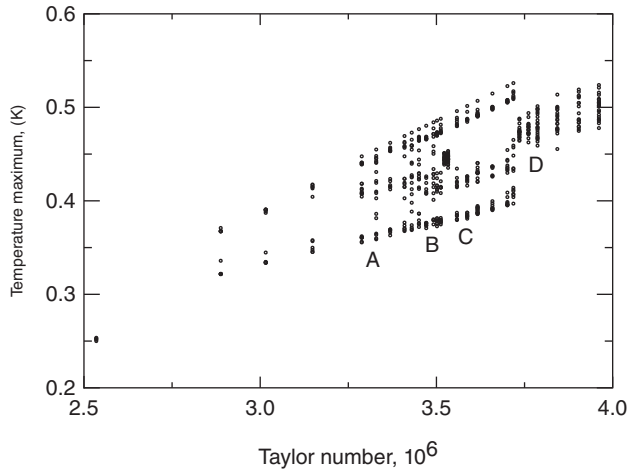

Figure 1.12. Bifurcation diagram showing the maxima of $m = 2$ temperature amplitudes at successive values of $\mathcal{T}$ keeping Θ constant at $\Theta \simeq 1.75$. Adapted from *Young and Read* [2008]. Copyright 2008 with permission from Elsevier.

where σ, r_a, and b are constants, X is related to $A(\tau)$, Y is related to $V(\tau)$ and $Z \sim F(A, V)$ [e.g., *Brindley and Moroz*, 1980; *Gibbon and McGuinness*, 1980; *Pedlosky and Frenzen*, 1980; *Klein*, 1990], which is the famous set of equations that can result in the Lorenz attractor [*Lorenz*, 1963a]. In the presence of a "planetary vorticity gradient" or β effect, the wave-zonal flow interaction problem may reduce to a set analogous to the *complex* Lorenz equations [e.g., *Gibbon and McGuinness*, 1980; *Fowler et al.*, 1982; *Lovegrove et al.*, 2001, 2002]:

$$\frac{dX}{d\tau} = \sigma(Y - X), \tag{1.18}$$

$$\frac{dY}{d\tau} = XZ + r_a X - aY, \tag{1.19}$$

$$\frac{dZ}{d\tau} = \frac{1}{2}(X^* Y + XY^*) - bZ, \tag{1.20}$$

where X and Y are now complex variables and r_a and a are complex parameters. The onset of chaos in these models as parameters are smoothly varied is characterized by a particular sequence of transitions typically involving either a sudden "snap-through" bifurcation from an initially steady wave as dissipation is reduced or a period-doubling cascade from an "amplitude vacillation" state as dissipation is increased [*Klein*, 1990].

In the thermal annulus, the situation seems more complicated, with the possibility of at least two distinct routes to chaotic behavior. In one case, periodic AV gives way to an azimuthally asymmetric, chaotically modulated vacillation in which two or more adjacent wave numbers occur in irregular competition. The final "chaotic" state appears to comprise at least three independent frequencies together with a "noisy" component associated with

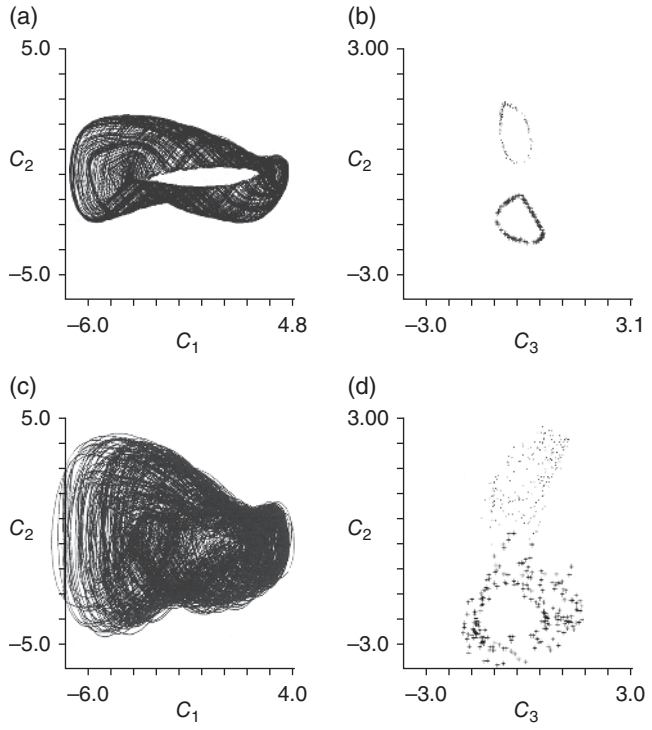

Figure 1.13. Phase portraits [(a) and (c)] and Poincaré sections [(b) and (d)] obtained from measurements of temperature in a rotating annulus showing a transition from amplitude vacillation (top) to a chaotic "modulated amplitude vacillation" (bottom). Adapted from *Read et al.* [1992] with permission.

the observed "chaos" [*Read et al.*, 1992; *Früh and Read*, 1997]. The transition may be illustrated in reconstructed phase portraits derived from time series of temperature measurements, for example. Examples are illustrated in Figure 1.13 from the experiments reported by *Read et al.* [1992]. The other main route may be via the period-doubling sequence found in model simulations by *Young and Read* [2008] although, as mentioned above, this route has so far proved elusive in real experiments.

1.3.6. Structural Vacillation and Transition to Geostrophic Turbulence

"Structural vacillation" (also known as "shape" or "tilted-trough vacillation" or SV [*White and Koschmieder*, 1981; *Buzyna et al.*, 1984]) occurs as the irregular flow transition is approached and, in its purest expression, is characterized by a nearly periodic, horizontal tilting of the radial axes of wave peaks and troughs [*Weng et al.*, 1986; *Weng and Barcilon*, 1987]. However, in practice it takes many different forms, depending upon a variety of factors, including how close the dominant wave number m may be to Hide's maximum stable wave number $m_{\max}$ [cf. equation (1.13)]. This becomes more pronounced as

Ω is increased, until the regular flow pattern breaks down into fully irregular flow [*Pfeffer et al.*, 1980; *Buzyna et al.*, 1984].

In its "purest" form, SV has been observed as the periodic tilting back and forth of the main wave troughs. In association with this observation, the lateral distribution of eddy energy within the wave was observed to shift back and forth between the inner and outer sides of the channel. This observation led some to suggest a kinematic form for the wave as the superposition of dominant waves with the same zonal wave number and with lateral structures

$$\phi_1(y) = A_1 \sin \pi y, \tag{1.21}$$

$$\phi_2(y) = A_2 \sin 2\pi y, \tag{1.22}$$

both propagating azimuthally at different phase speeds.

This type of behavior has been reproduced in a class of simple, low-order numerical models in which a small number of wave modes are allowed to interact through mutual advection in a quasi-geostrophic model. *Weng and Barcilon* [1987], for example, followed a much earlier approach pioneered by *Lorenz* [1963b] and applied it to a nonlinear version of the Eady model including the first two lateral modes (cf. equations (1.21) and (1.22)) to obtain solutions in which eddy energy oscillated in y through nonlinear interference between the two gravest y modes with the same x wave number (e.g., see Figure 1.14).

In practice, however, observed 'structural vacillations' are often more complicated than this picture would suggest, for example, with transient small-scale features growing and decaying within a large-scale pattern dominated by a single azimuthal wave number. Oscillations often appear to be strongly intermittent and irregular, and the phenomenon suggests the growth of small-scale instabilities within the large-scale pattern (either barotropic or baroclinic) that do not reach sufficient amplitude to disrupt the main pattern. *Read et al.* [1992] found that the onset of SV occurs quite suddenly at a well-defined point in parameter space, again with evidence of intermittency in time. The irregular character of the oscillations becomes steadily more apparent as Ω is increased, and the large-scale pattern becomes gradually more distorted until it begins to break up into irregular flow. This does not seem to be readily consistent with notions of chaos in the formal sense, and its precise nature is still not fully understood (see *Read et al.* [1992] for further discussion). SV is frequently regarded as an intermediate state prior to the full onset of irregular wave flow or "geostrophic turbulence."

At the highest rotation rates, the wave number spectrum is observed to fill up to become a broadband continuum, though a limited band of wave numbers still tends to dominate the spectrum. The most detailed laboratory measurements of the transition to irregular flow with

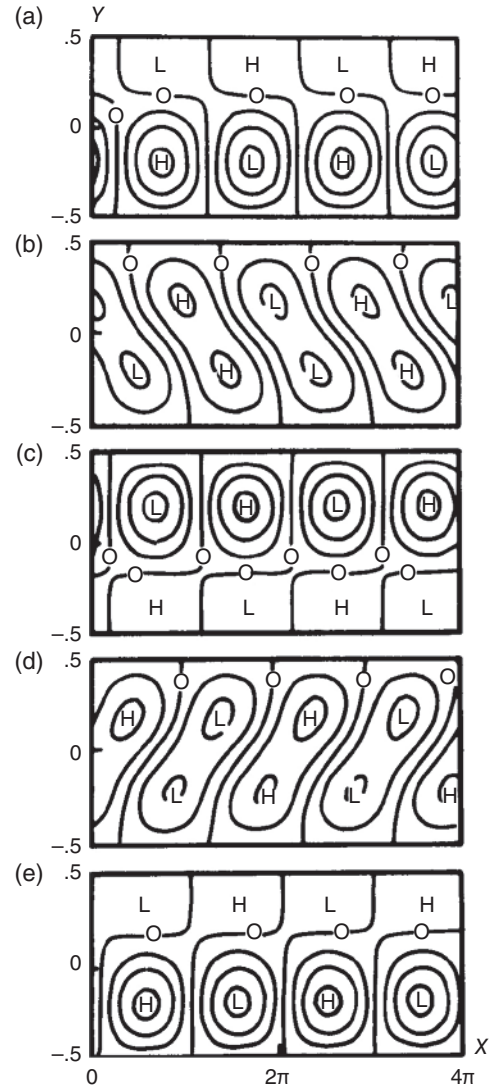

Figure 1.14. Stream function fields from a wave number 6 flow at mid-depth in the $x-y$ plane of a zonal channel (where x is the zonal direction and y the lateral or meridional direction) during a structural vacillation cycle, as obtained in a low-order quasi-geostrophic model. Adapted from *Weng and Barcilon* [1987] with permission of John Wiley & Sons, Inc.

increasing Ω were carried out by *Buzyna et al.* [1984] [see also *Pfeffer et al.*, 1980] and *Hide et al.* [1977], in the former case using the large annulus at Florida State University. Both studies showed the gradual broadening of the wave number spectrum and increasing significance of nonharmonically related azimuthal components as the fully developed irregular regime was entered (some examples from the study by *Buzyna et al.* [1984] are shown in Figure 1.15). At extreme parameter values, the time-averaged spectrum does not display strong peaks at any particular individual wave number but appears as a broad

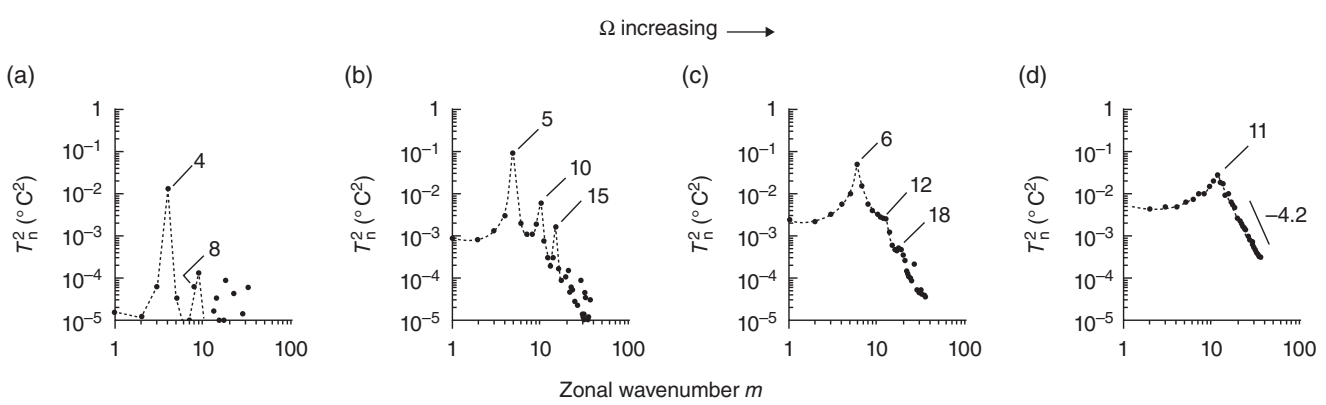

Figure 1.15. Azimuthal wave number power spectra obtained from measurements of temperature in a rotating annulus as Ω is increased through the regular wave regime toward fully developed "geostrophic turbulence". Experiments were carried out at the following points in $(\Theta, \mathcal{T})$ parameter space: (a) 1.44, 1.30×10^8, (b) 0.344, 5.40×10^8, 0.230, 8.07×10^8, and (d) 0.086, 2.16×10^9. Adapted from *Buzyna et al.* [1984] with permission.

continuum with maximum power over a range of relatively low wave numbers dominated by the main baroclinic wave activity with a characteristic quasi-power law decay toward the highest wave numbers that commonly approached $k^{-3} - k^{-4}$ [*Hide et al.*, 1977; *Pfeffer et al.*, 1980; *Buzyna et al.*, 1984] and even steeper in some cases [*Pfeffer et al.*, 1980; *Buzyna et al.*, 1984]. Simple heuristic arguments based on the Kolmogorov-Kraichnan theory [*Kraichnan*, 1967, 1971] predicts energies to decay as k^{-3} at high wave numbers in an enstrophy-dominated inertial range, but this is not the only possible explanation. The (possibly transient) formation of sharp fronts and vorticity filaments within geostrophically turbulent flows may lead to a kinetic energy spectrum with a slope as steep as k^{-4} [e.g., *Saffman*, 1971; *Brachet et al.*, 1988]. The formation of persistent, stable vortex structures within geostrophically turbulent flows can also perturb the simple Kolmogorov-Kraichnan scaling arguments by introducing some spatiotemporal intermittency to the flow. This effect can also apparently lead to spectral slopes of $k^{-3} - k^{-4}$ or even steeper [e.g., *Basdevant et al.*, 1981; *McWilliams*, 1984], although the presence of imposed vorticity gradients (e.g., due to a β effect or topography) may weaken such eddies and the flow reverts toward a k^{-3} energy spectrum.

A further question regarding these highly turbulent flows with strong background rotation is whether they also exhibit any evidence for an inverse energy cascading inertial range. Early theoretical work and models [e.g., *Salmon*, 1978; *Rhines*, 1979; *Salmon*, 1980] suggested that such inverse cascades would be relatively common in stratified, quasi-geostrophic flows, with energy being injected into the barotropic mode at around the internal Rossby deformation radius via baroclinic self-interactions, leading to a $K_3^{-5/3}$ inertial range (where K_3 is the three-dimensional total wave number) if a sufficient scale separation exists between energy injection and large-scale dissipation and forcing. The existence or otherwise of an inverse energy cascade in Earth's atmosphere or oceans continues to be an area of active controversy, with recent work suggesting that energy cascades upscale from around the first internal baroclinic deformation radius toward larger scales in the oceans [*Scott and Wang*, 2005; *Scott and Arbic*, 2007], though without a $k^{-5/3}$ inertial range apparent (at least in the sea surface height signature in satellite altimetric measurements). The development of coherent structures at large scales in the atmosphere, however, has been suggested to lead to a suppression of spectrally local nonlinear interactions and consequently the suppression of any significant inverse energy cascade at scales larger than the main energy-containing baroclinic scales in the atmosphere [e.g. *Schneider and Walker*, 2006; *O'Gorman and Schneider*, 2007].

Such issues were not considered in earlier experimental studies [*Hide et al.*, 1977; *Pfeffer et al.*, 1980; *Buzyna et al.*, 1984; *Bastin and Read*, 1997, 1998], which only presented and discussed basic temperature variance spectra and synoptic structures from their measurements. As is evident from Figure 1.15, such spectra show little obvious evidence of the $K_3^{-5/3}$ inertial range that might indicate an energy-dominated cascade at low wave numbers. *Wordsworth et al.* [2008] did explore aspects of spectral energy transfers in a set of rotating annulus experiments, both with and without sloping horizontal boundaries, even though such experiments also showed no obvious sign of the classical $K_3^{-5/3}$ inertial range. Nevertheless, these experiments did show evidence for a weak, spectrally local (eddy-eddy) upscale kinetic energy cascade in

the presence of sloping boundaries and a much stronger direct (spectrally nonlocal) upscale energy transfer into the zonally symmetric component of the flow, in extreme cases deforming the large-scale baroclinic zonal flow into a pattern of multiple parallel jets and baroclinic zones. Such patterns had been anticipated in several earlier studies [*Mason*, 1975; *Bastin and Read*, 1997, 1998], which also noted the tendency to form flows with complex radial structures, but these did not examine the energy exchanges in such detail.

However, this whole subject area relating to energy exchanges in geostrophically turbulent or chaotic flows is substantially underexplored and deserves further intensive study in future research. The respective roles of baroclinic and barotropic energy exchanges (both kinetic and potential) remain uncertain in the general case, and how such roles scale and vary with key control parameters is virtually unknown. The study by *Wordsworth et al.* [2008] only considered quasi-barotropic energy exchanges in detail in the cases they were able to measure, though they attempted to infer some aspects of the baroclinic-barotropic exchanges indirectly. But a more detailed study utilizing combinations of velocity and temperature measurements with good spatial coverage and high spatial resolution are really needed to elucidate some of the most challenging outstanding questions, that are currently major issues for understanding the global circulation of both the atmosphere and oceans [cf *Schneider and Walker*, 2006; *Zurita-Gotor and Lindzen*, 2007; *Jansen and Ferrari*, 2012].

1.4. HEAT TRANSPORT AND ROLE OF BAROCLINIC WAVES

It is often asserted [e.g., *Hide and Mason*, 1975] that baroclinic annulus waves develop from a baroclinically unstable background state and serve primarily to transfer heat upward and horizontally from hot regions toward cooler ones. But heat transfer within the baroclinic rotating annulus is actually significantly more complicated than this would suggest.

If the annulus were filled with a conducting solid instead of a fluid, heat would only be transferred by molecular conduction. Hence, with isothermal vertical boundaries the equilibrated isotherms would lie on cylindrical surfaces coaxial with the axis of symmetry. Such a configuration in a fluid would be very unstable, however, since large amounts of potential energy would be stored compared with the lowest energy state that could be obtained by an adiabatic rearrangement of the fluid to place the denser fluid as low as possible (and vice versa). Where the boundary temperatures are actively maintained, however, the complete adiabatic rearrangement of the fluid to its lowest potential energy state is not sustainable but results in a residual buoyancy-driven overturning circulation, mainly confined to thin boundary layers adjacent to the vertical boundaries (provided the Rayleigh number is large enough; see below). Figure 1.16 shows an example from a numerical simulation of the equilibrated flow in a nonrotating fluid annulus. This clearly shows the temperature field assuming a bottom-heavy configuration away from the vertical boundaries but with complex thermal structure adjacent to the sidewalls as the temperature adjusts to the isothermal boundary conditions within complex sidewall boundary layers. Some of this structure is associated with the strong overturning circulation within the sidewall boundary layers, where conductive heating/cooling is balanced by (mainly vertical) advection of heat, with a return flow in the (quasi-inviscid) interior. The interior flow redistributes hot and cold fluid until it reaches a state of minimum potential energy, i.e., with as much as possible of the cold dense fluid at the bottom of the cavity. Hence, isotherms in the interior become virtually horizontal and stably stratified in the vertical, adjusting to become vertical in thin conduction-dominated boundary layers adjacent to the sidewalls. In this state, advective heat transport (by laminar flow) is

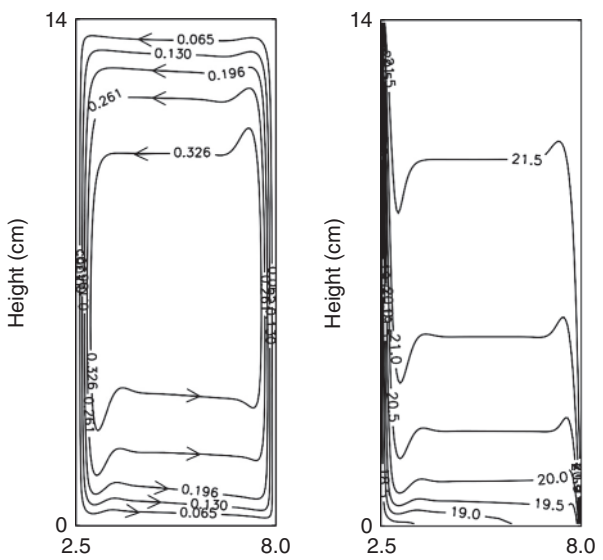

Figure 1.16. Numerical simulation of the equilibrated axisymmetric flow in a rotating annulus experiment with sidewalls maintained at different temperatures but with $\Omega = 0$: (a) stream function for the meridional circulation in the (r, z) plane; (b) corresponding temperature field with thin thermal boundary layers adjacent to each sidewall.

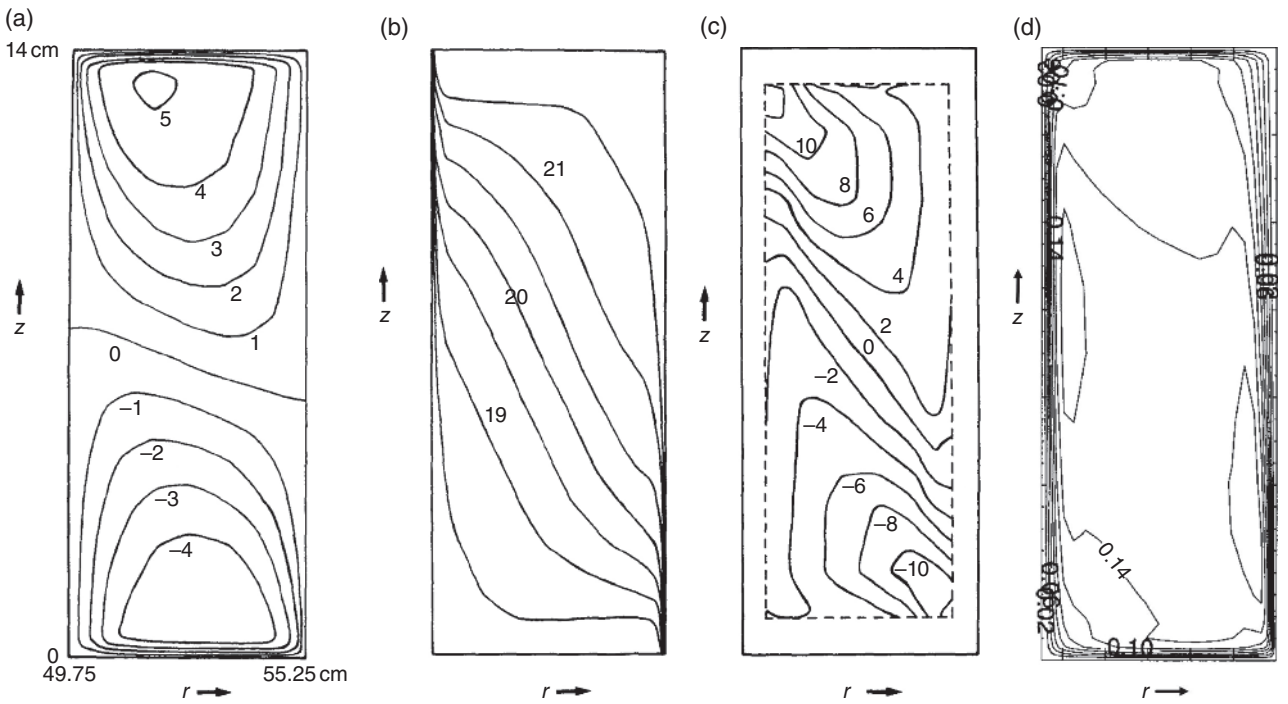

Figure 1.17. Cross sections in the (r, z) plane of (a) azimuthal velocity (mm/s), (b) temperature (°C), (c) radial gradient of QG potential vorticity (s^{-1}) (computed by *Bell and White* [1988]), and (d) meridional stream function (cm^2/s^1) in the axisymmetric regime of a rotating annulus subject to differential heating at the sidewalls. (Adapted from *Read* [2003] with permission.)

apparently as efficient as possible as measured by the nondimensional Nusselt ($\mathcal{N}$) or Péclet (Pe) numbers

$$\mathcal{N} = \frac{\text{Total heat transport}}{\text{Heat transport by conduction alone}}, \tag{1.23}$$

$$\text{Pe} = \frac{\text{Advective heat transport}}{\text{Heat transport by conduction alone}}. \tag{1.24}$$

When the system is rotated, Coriolis accelerations begin to influence the circulation, deflecting horizontal radial motion into the azimuthal direction. The axisymmetric flow at low values of Ω is therefore similar to the nonrotating case, except (a) an azimuthal component of flow is induced, producing jets antisymmetric about middepth (for identical upper and lower boundary conditions), prograde at the top (where radial flow is inward) and retrograde below (where radial flow is outward), and (b) radial flow becomes largely confined to Ekman layers adjacent to the horizontal boundaries (for Ω sufficiently large). When Coriolis accelerations dominate the interior flow, any $O(1)$ radial flow has to be geostrophic, requiring an azimuthal pressure gradient. Such a gradient cannot occur in an axisymmetric circulation unless a rigid meridional barrier is present, so radial flow strong enough to carry significant amounts of heat energy across the annulus becomes largely confined to the Ekman layers. This is clearly seen in the temperature and stream function fields of the rotating, axisymmetric flow illustrated in Figure 1.17a and 1.17d. Meanwhile, the azimuthal flow assumes a form where geostrophic balance applies except in the Ekman layers, within which viscous accelerations dominate.

Since the radial flow becomes confined to Ekman layers when $\Omega \neq 0$, the efficiency of advective heat transport is governed primarily by the mass transport, which can be accommodated within an Ekman layer. For a given geostrophic zonal flow in the interior, the advective Ekman transport is proportional to the depth of the Ekman layer (i.e., proportional to $V\mathcal{E}^{1/2}$, where $\mathcal{E}$ is the Ekman number and V the azimuthal velocity scale; see below). Since $\mathcal{E}$ is inversely proportional to Ω, the efficiency of advective heat transport must decrease with Ω given a constant ΔT, V is proportional to Ω^{-1}, and Ekman transport is proportional to $\Omega^{-1}\mathcal{E}^{1/2} \propto \Omega^{-3/2}$. Thus, as Ω increases, advective heat transport must decrease. Such a decrease is clearly apparent in Figure 1.18, which shows a compilation of both laboratory measurements of Nusselt number and from numerical simulations [*Read*, 2003; *Pérez*, 2006]. The variation of Nusselt number $\mathcal{N}$ in a pure axisymmetric flow in which baroclinic waves are suppressed is indicated by diamonds, which broadly confirm the decay as $\Omega^{-3/2}$, though note

that this scaling applies more precisely to the Péclet number Pe (= $\mathcal{N} - 1$; see equation (1.24)), which decays more rapidly with Ω toward zero than $\mathcal{N}$ (which decays toward $\mathcal{N} = 1$). Since conductive heat transport is always present and is unaffected by rotation, the resultant thermal field becomes increasingly dominated by conduction. Hence, the isotherm structure will tend toward the vertical alignment characteristic of the conductive state as Ω increases. It is reasonable, therefore, for waves to develop in such a flow provided they are able to transfer heat radially in the interior, which is possible in a geostrophically balanced rotating fluid since waves are associated with a periodically varying azimuthal pressure gradient to balance a radial geostrophic flow.

Laboratory experiments show that such wavelike disturbances with these properties will frequently develop under many circumstances, with the primary role of transferring heat and releasing "available" potential energy. When such waves are present, experiments have consistently demonstrated that they increase the effectiveness of advective heat transfer quite significantly. The experimental measurements and simulations represented in Figure 1.18 show this effect very clearly, more or less maintaining the total Nusselt number of the whole system at a value close to its nonrotating value. Such an effect has been noted since the early work of *Bowden* [1961] and *Bowden and Eden* [1965], though a fully quantitative, theoretical understanding of this has remained elusive.

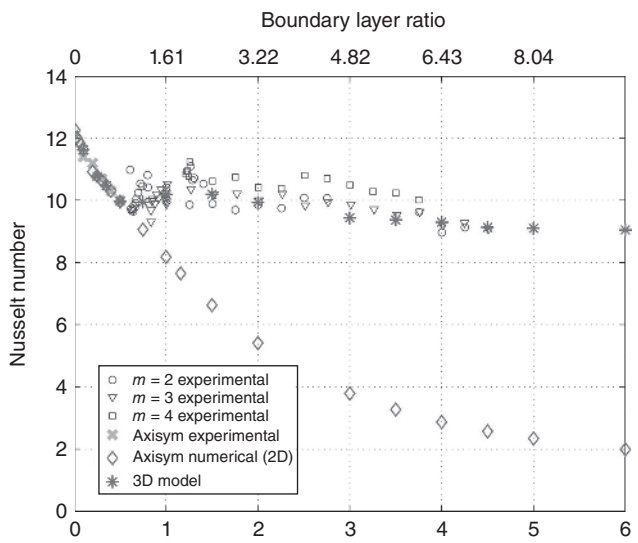

Figure 1.18. Experimental and numerically simulated total heat transport (Nusselt number) in a rotating annulus experiment using data from *Read* [2003] and *Pérez* [2006]. Both 2D and 3D models were used for the numerical simulations. (See key inside the figure for a description of each measurement.)

1.4.1. Eddy Heat Transfer in Oceans and Atmospheres

Note that the above arguments will apply in a qualitative sense to a planetary atmosphere save that the state to which the thermal structure relaxes in the absence of (large-scale) fluid motion is one not of conductive equilibrium but of radiative (or radiative-convective) equilibrium [e.g., *Pierrehumbert*, 2010]. This would suggest that parameters measuring the efficiency of atmospheric heat transport, such as the Nusselt number $\mathcal{N}$, need to be redefined, for example, with respect to a radiative-convective equilibrium state rather than a pure conductive one. In the case of Earth, pure radiative-convective equilibrium would result in a temperature contrast between equator and poles of ~150 K, instead of ~60 K observed on average [e.g., *Andrews et al.*, 1987], indicating the dominant role of dynamical advective heat transport in the atmosphere. Similar considerations may apply in the oceans, for which parameterization of baroclinic eddy transports are of particular importance. This is because the scales of baroclinic instability are so much smaller than the domain scale of an ocean basin that they are extremely difficult and/or expensive to resolve adequately in ocean circulation numerical models.

Various approaches toward the parameterization of eddy transports have been developed over many years for this purpose [e.g., *Plumb and Mahlman*, 1987; *Gent and McWilliams*, 1990; *Gent et al.*, 1995; *Treguier et al.*, 1997; *Killworth*, 1997; *Visbeck et al.*, 1997; *Marshall and Adcroft*, 2010]. A major advance in the development of such parameterizations that forms the basis of many contemporary schemes in current use in ocean models derives from the work of *Gent and McWilliams* [1990] and *Gent et al.* [1995]. Here an "eddy-induced" or "bolus" velocity is introduced that advects temperature and other tracers in such a manner as to flatten density surfaces. The original scheme proposed by *Gent and McWilliams* [1990] derived such an eddy-induced velocity from a parameterization of buoyancy fluxes that were assumed to act diffusively down- gradient with respect to the ambient (e.g., zonal mean) buoyancy field in the form (suitable for a zonally reentrant domain):

$$u^* = -\frac{\partial}{\partial z}\left(\frac{\overline{u'\rho'}}{\partial\overline{\rho}/\partial z}\right) \tag{1.25}$$

$$= -\frac{\partial \chi^*_{\mathrm{GM}}}{\partial z}, \tag{1.26}$$

$$w^* = \frac{\partial}{\partial y}\left(\frac{\overline{u'\rho'}}{\partial\overline{\rho}/\partial z}\right) \tag{1.27}$$

$$= \frac{\partial \chi^*_{\mathrm{GM}}}{\partial y}. \tag{1.28}$$

Here the term in parentheses on the right-hand sides of each of equations (1.25) and (1.27) is effectively the stream function χ^*_{GM} for the eddy-induced azimuthal mean flow (u^*, w^*) in the meridional (r, z) plane. *Gent and McWilliams* [1990] proposed that the buoyancy flux in this definition of χ^* be parameterized as a down-gradient diffusion of zonallyaveraged buoyancy

$$\chi^*_{\mathrm{GM}} = \left(\frac{\overline{u'\rho'}}{\partial\overline{\rho}/\partial z}\right) = -\left(\mathcal{K}\frac{\partial\overline{\rho}/\partial y}{\partial\overline{\rho}/\partial z}\right), \tag{1.29}$$

where $\mathcal{K}$ is a suitably defined eddy diffusion coefficient that needs to be completed with a suitable closure model. The latter is commonly assumed to take the general form

$$\mathcal{K} = \alpha L_{\mathrm{eddy}} U_{\mathrm{eddy}}, \tag{1.30}$$

where L_{eddy} and U_{eddy} are characteristic scales for eddy length and velocity scales and α is a dimensionless constant, found empirically to require a value $O(10^{-2})$ [e.g., *Visbeck et al.*, 1997; *Marshall and Adcroft*, 2010].

There remains significant uncertainty, however, as to the physical basis for choosing L_{eddy} and U_{eddy}. L_{eddy} represents a prescribed "mixing length", suggestions for which have included either the so-called-Rhines scale $L_{\mathrm{Rhines}} = (U_{\mathrm{rms}}/\beta)^{1/2}$ [*Larichev and Held*, 1995; *Treguier et al.*, 1997], the width of the baroclinic zone [*Green*, 1970; *Visbeck et al.*, 1997], or the Rossby deformation radius [*Stone*, 1972]. U_{eddy} has been taken variously as either a "typical" thermal wind scale related to the zonal mean horizontal thermal gradient [*Green*, 1970] or setting $U_{\mathrm{eddy}} \sim L_{\mathrm{eddy}}/\tau_{\mathrm{eddy}}$, where τ_{eddy} is a "typical" eddy overturning time scale that might be derived, for example, from linear baroclinic instability theory [*Stone*, 1972; *Haine and Marshall*, 1998] or weakly nonlinear theory [*Pfeffer and Barcilon*, 1978; *Read*, 2003]. In addition, problems may arise if a parameterization scheme fails to respect key conservation principles, especially energy and potential vorticity [e.g., *Marshall and Adcroft*, 2010]. The parameterization of the eddy-driven "bolus" velocity from zonal mean fields is another controversial issue since it is not always clear that the horizontal eddy buoyancy flux necessarily acts diffusively down gradient with respect to the zonal mean buoyancy field [e.g., *Treguier et al.*, 1997; *Marshall and Adcroft*, 2010]. *Treguier et al.* [1997] and *Killworth* [1997] suggested an alternative approach based on assuming that potential vorticity is more generally diffused down gradient than pure buoyancy such that the eddy-induced velocity (u^*, w^*) is defined as

$$u^*_{\mathrm{THL}} = -\frac{\partial}{\partial z}\left(\frac{\overline{u'\rho'}}{\partial\overline{\rho}/\partial z}\right) \tag{1.31}$$

$$\simeq -\frac{\overline{u'q'}}{f} \simeq \frac{\mathcal{K}(y,z)\partial\overline{q}/\partial r}{f} \tag{1.32}$$

$$= -\frac{\partial\chi^*_{THL}}{\partial z}, \tag{1.33}$$

$$w^*_{\mathrm{THL}} = \frac{\partial\chi^*_{THL}}{\partial y}, \tag{1.34}$$

where $\mathcal{K}_q(y,z)$ is again a suitably defined eddy diffusion coefficient, this time for potential vorticity q, and is assumed here to be variable in space.

A complete understanding of all of these issues therefore remains elusive, and there remains a continuing problem of how to verify any scheme of parameterization with the desired degree of rigor. In this respect, laboratory experiments such as the rotating, thermally driven annulus ought to have something important to contribute. Experimental techniques have been available for some time to measure both the total heat transport across the annular cavity (e.g., via calorimetric methods to determine the total heat transport across a given sidewall boundary) *and* the interior eddy variances and fluxes of heat, momentum, and vorticity associated with baroclinic waves. The quantitative interpretation of these measurements, however, requires a clear understanding of the various mechanisms at work within rotating annulus circulations to transport heat energy across the annular channel. These include direct thermal conduction and direct overturning circulations (mainly in boundary layers) as well as macroturbulent transports by baroclinic eddies themselves. In subsequent sections, therefore, we examine and review the main boundary layer and eddy processes that contribute to heat transport in the annulus, culminating in some preliminary attempts to apply an analogue of ocean baroclinic eddy parameterization schemes within an axisymmetric numerical annulus model in which baroclinic instability is artificially suppressed.

1.4.2. Regimes of Axisymmetric Flow: Heat and Momentum Transport

Although the description of the axisymmetric flow in the introduction to this section gave a plausible explanation for the observed axisymmetric and wave regimes in the annulus, it is a highly simplified discussion that glosses over more subtle aspects of the problem. In this section, we take a more quantitative view of the axisymmetric flow in the annulus to put the above discussion onto a stronger theoretical footing and as an illustration of the use of scale analysis and boundary layer theory.

Early analyses [*McIntyre*, 1968; *Sugata and Yoden*, 1992] followed the scaling approach developed by *Gill* [1966], which *Hignett et al.* [1981] and *Hignett* [1982] further extended for an incompressible Boussinesq fluid in a rotating annulus of vanishingly small relative curvature $(2[b-a]/[b+a] \ll 1$, so one may use Cartesian geometry)

and neglected centrifugal accelerations. It is convenient to define a meridional stream function χ such that

$$u = \frac{\partial \chi}{\partial z}, \qquad v = -\frac{\partial \chi}{\partial x}. \tag{1.35}$$

The steady-state equations for momentum, continuity, and heat then reduce to a zonal momentum equation

$$\nu \nabla^2 v = f \frac{\partial \chi}{\partial z} + J(v, \chi), \tag{1.36}$$

where $f = 2\Omega$ and the Jacobian is defined as

$$J(c, d) = \frac{\partial c}{\partial x}\frac{\partial d}{\partial z} - \frac{\partial c}{\partial z}\frac{\partial d}{\partial x}; \tag{1.37}$$

the azimuthal vorticity equation is

$$\nu \nabla^4 \chi = g\alpha \frac{\partial T}{\partial x} - f\frac{\partial v}{\partial z} - J(\chi, \nabla^2 \chi), \tag{1.38}$$

where T is the temperature and α the volumetric expansion coefficient and vorticity ζ is defined as

$$\zeta = \frac{\partial u}{\partial z} - \frac{\partial v}{\partial x} = \nabla^2 \chi; \tag{1.39}$$

and the temperature equation is

$$\kappa \nabla^2 T + J(\chi, T) = 0. \tag{1.40}$$

We consider a container of aspect ratio ϵ defined by

$$\epsilon = \frac{H}{L} \tag{1.41}$$

(where H and L are the vertical and horizontal length scales, respectively, of the domain) and apply boundary conditions

$$\chi = \frac{\partial \chi}{\partial z} = v = \frac{\partial T}{\partial z} = 0, \quad z = 0, H, \tag{1.42}$$

$$\chi = \frac{\partial \chi}{\partial x} = v = T - T_0 = 0, \quad x = -L/2, +L/2. \tag{1.43}$$

We make use of dimensionless parameters such as the Ekman number $\mathcal{E}$ defined by

$$\mathcal{E} = \frac{\nu}{\Omega H^2}, \tag{1.44}$$

the Prandtl number $\mathrm{Pr}(= \sigma/\kappa)$, and the Rayleigh number

$$\mathrm{Ra} = \frac{g\alpha \Delta T L^3}{\kappa \nu}. \tag{1.45}$$

It is also convenient to define Nusselt ($\mathcal{N}$) and Péclet (Pe) numbers as measuring the ratios of total heat transport and advective heat transport, respectively, to that due to conduction, which we take to be

$$\mathcal{N} = \frac{\Xi}{\kappa} + 1 = \mathrm{Pe} + 1 \tag{1.46}$$

(where Ξ is a characteristic scale for χ). We then carry out a scale analysis with the aim of deriving the dominant dynamical balances in the interior and principal boundary layers and obtain the dependence of $\mathcal{N}$ and the zonal velocity scale on external parameters over as wide a range as possible. Initial assumptions are restricted as follows:

(i) Aspect ratio ϵ is not too different from unity.

(ii) Single thickness scales are assumed, ℓ for the side and h for the horizontal boundary layers.

(iii) Outside the boundary layers there is a distinct interior flow with length scales L and H such that $(\ell, h) \ll (L, H)$.

(iv) Prandtl number $\mathrm{Pr} \gg 1$.

1.4.2.1. Nonrotating Problem. We assume the flow to comprise an advective interior and thin sidewall boundary layers and nondimensionalize in the thin sidewall layer of thickness ℓ using

$$\Delta x = \ell \Delta x^*, \quad \Delta z = H \Delta z^*, \quad T - T_o = \Delta T T^*, \quad \chi = \Xi \chi^*. \tag{1.47}$$

Thus equation (1.40) becomes

$$\nabla^2 T^* + \frac{\Xi \ell}{\kappa H} J(\chi^*, T^*). \tag{1.48}$$

For advective/diffusive balance, we require

$$\Xi = \frac{\kappa H}{\ell}. \tag{1.49}$$

For this case, (1.38) becomes

$$\nabla^4 \chi^* = \mathrm{Ra}\left(\frac{\ell}{L}\right)^4 \frac{\partial T^*}{\partial x^*} - \frac{1}{\mathrm{Pr}} J(\chi^*, \nabla^2 \chi^*). \tag{1.50}$$

If $\mathrm{Pr} \gg 1$, we obtain a buoyancy/viscous balance in the sidewall boundary layer, implying that

$$\ell = \mathrm{Ra}^{-1/4} \epsilon^{1/4} L, \tag{1.51}$$

which was the result obtained by *Read* [1992] [see also *Fein*, 1978; *Friedlander*, 1980] for the principal boundary layer scale when $N^2 \mathrm{Pr}/f^2 \gg \mathcal{E}^{2/3}$. In this case, the Nusselt or Péclet number is obtained from equation (1.49) as

$$\mathcal{N} - 1 = \mathrm{Pe} = \frac{\Xi}{\kappa} = O\left[\mathrm{Ra}^{1/4} \epsilon^{3/4}\right]. \tag{1.52}$$

1.4.2.2. Effects of Rotation. In considering the relative impact of rotation on the circulation, it seems intuitive that the Ekman layer will be of importance. It is therefore convenient to follow an approach due to *Hignett et al.* [1981] and recently applied to good effect in the context of convection in rotating systems by *King et al.* [2009] and *King et al.* [2012] in defining a parameter $\mathcal{P}$ measuring the (square of the) ratio of the thickness of the Ekman layer and sidewall buoyancy layer. Thus

$$\mathcal{P} = \mathrm{Ra}^{-1/2} \mathcal{E}^{-1}, \tag{1.53}$$

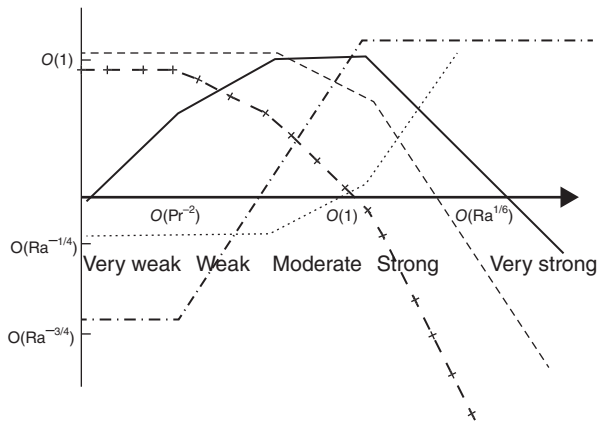

Figure 1.19. Schematic diagram showing the dependence of derived parameters on internal parameters in the various axisymmetric regimes defined in terms of $\mathcal{P}$ assuming $\epsilon = O(1)$. Quantities represented are $VL/(\kappa \mathrm{Ra}^{1/2})$ (solid line); $\Xi/(\kappa \mathrm{Ra}^{1/4})$ (dashed line); γ (dash-dotted line); ℓ/L (dotted line), and Ro (dash-crossed line). (Adapted from *Read* [1986] with permission).

(assuming hereafter for simplicity that $\epsilon = 1$) which is proportional to Ω. Based on a consideration of the full range of $\mathcal{P}$, we can effectively identify up to six distinct regimes of axisymmetric flow (see also Figure 1.19):

(i) No rotation, $\mathcal{P} = 0$.
(ii) Very weak rotation, $0 \ll \mathcal{P} \ll \mathrm{Pr}^{-2}$.
(iii) Weak rotation, $\mathrm{Pr}^{-2} \ll \mathcal{P} \ll 1$.
(iv) Moderate rotation, $\mathcal{P} \simeq 1$.
(v) Strong rotation, $1 \ll \mathcal{P} \ll \mathrm{Ra}^{1/6}$.
(vi) Very strong rotation, $\mathcal{P} \gg \mathrm{Ra}^{1/6}$.

We now briefly outline their characteristics:

(i) No rotation: This has already been discussed above in Section 1.4.2.1, with consequent scales for ℓ and Pe. Note that we can obtain an estimate of isotherm slope $\gamma = \Delta T_h/\Delta T$ (where ΔT_h is the horizontal temperature contrast) from a consideration of the balances in the zonal vorticity equation. Provided $\mathrm{Pr} \gg 1$, a buoyancy/viscous balance holds in the interior, so that

$$g\alpha\, \partial T/\partial x = O(g\alpha \Delta T \gamma/L) \tag{1.54}$$

$$= \nu \nabla^4 \chi (= O(\nu \Xi L^{-4}). \tag{1.55}$$

Hence $\gamma < \mathrm{Ra}^{-3/4} \ll 1$ and isotherms are quasi-horizontal.

(ii) Very weak rotation: When f is no longer zero, (1.36) is coupled to (1.38) and gyroscopic torques render v non-zero. We obtain an estimate for the zonal velocity scale V by scaling (1.38) in the Ekman layer using its characteristic depth $h = \mathcal{E}^{1/2} L$. Hence, (1.36) becomes

$$\mathrm{Pr}\mathcal{P}^{1/2} \nabla^2 v^* = \frac{fL}{V} \frac{\partial \chi^*}{\partial z^*} + J(v^*, \chi^*). \tag{1.56}$$

Thus, for $\mathcal{P} \ll \mathrm{Pr}^{-2}$ we have an inertial/Coriolis balance in the Ekman layer (i.e., there is no proper Ekman layer), and the entire flow is characterized by local conservation of angular momentum [hence $V = O(fL)$, which is proportional to $\mathcal{P}$; see Figure 1.19].

(iii) Weak rotation: For $\mathcal{P} \gg \mathrm{Pr}^{-2}$, the viscous term in (1.56) becomes dominant in the Ekman layer (i.e., normal Ekman layers exist), thus rescaling V to $O(\kappa \mathrm{Ra}^{1/2} \mathcal{P}^{1/2}/L)$. This balance extends into the interior, while the previous balance in the sidewall layer is unchanged from regime (i). Despite the new scaling for V, the dominant balances (and scaling for Pe) in (1.40) also remain unchanged from (i). The rescaling of V does, however, affect the interior balance in the azimuthal vorticity equation, from a buoyancy/viscous balance to a buoyancy/Coriolis balance characteristic of the "thermal wind" balance typical of geostrophic flow. The reason why the (now geostrophic) scale for V does not go as Ω^{-1} typical of a thermal wind scale is because γ is now increasing rapidly with Ω ($\gamma = O(\mathcal{P}^{3/2})$), which more than outweighs the $\mathcal{P}^{-1}$ dependence of V for constant γ. Note also the zonal Rossby number $\mathrm{Ro} = V/fL = O(\mathrm{Pr}^{-1}\mathcal{P}^{-1/2}$ and is therefore $\ll 1$ (see Figure 1.19).

(iv) Moderate rotation: In this regime, the Ekman layer thickness is comparable with that of the sidewall buoyancy layer and so is expected to begin to exert a strong influence on the meridional circulation and transport. Anticipating that V will eventually tend toward the thermal wind scale $O(\mathcal{P}^{-1})$, this range of $\mathcal{P}$ delineates the regime where V reaches a maximum $V_o = O(\kappa \mathrm{Ra}^{1/2}/L)$. If the Ekman layer exercises dominant control over the radial mass transport, Ξ will be rescaled to $O(V_o L \mathrm{E}^{1/2}) = O(\kappa \mathrm{Ra}^{1/4} \mathcal{P}^{-1/2})$, implying a slow broadening of the sidewall advective/diffusive boundary layer from ℓ to $\ell \mathcal{P}^{1/2}$.

(v) Strong rotation: As $\mathcal{P}$ is increased beyond 1, the Ekman layers fully dominate the meridional circulation. By this point, the isotherm slope γ has become $O(1)$ and so cannot increase any further. Then V rescales to the familiar thermal wind scale $V = O(\kappa \mathrm{Ra}^{1/2} L^{-1} \mathcal{P}^{-1})$. The expansion of the advective/diffusive sidewall layer accelerates to $\ell' = O(\mathrm{Ra}^{-1/4} L \mathcal{P}^{3/2})$, extending the influence of thermal diffusion further into the interior. The heat transport Pe is rescaled to $O(\mathrm{Ra}^{1/4} \mathcal{P}^{-3/2})$, though it remains $\gg 1$ (see Figure 1.19).

(vi) Very strong rotation: In this final regime, the diffusive thermal sidewall layer expands to fill the interior and no separate thermal boundary layer and interior can be distinguished (though Stewartson $\mathcal{E}^{1/3}$ layers may exist in this limit). The critical value for $\mathcal{P}$ distinguishing regimes (v) and (vi) simply arises from equating ℓ' [see (v) above] with L so that $\mathcal{P} > \mathrm{Ra}^{1/6}$. All other balances remain unchanged from (v), i.e., the geostrophic interior and strong Ekman layers. Heat transport in this regime,

however, is dominated by thermal conduction so Pe $\rightarrow 0$ and $\mathcal{N} \rightarrow 1$.

1.4.2.3. Experimental Verification. The axisymmetric regimes discussed in Section 1.4.2.2 are capable (at least in principle) of existing in real systems given an experimental system operating in an appropriate parameter range. In practice, however, regimes (iv) – (vi) are not usually obtainable because of the development of nonaxisymmetric baroclinic waves within regime (iv) and beyond. This is consistent with the notion that baroclinic waves develop when Ekman layers begin to inhibit meridional heat transport.

An exception was provided by *Hignett* [1982], who made heat transport measurements in a rotating annulus with parallel sloping upper and lower endwalls that sloped strongly in the same sense as the isotherms. Such a configuration tends to inhibit the development of baroclinic waves (by constraining fluid trajectories away from the "wedge of instability"; [*Hide and Mason*, 1975; *Mason*, 1975]). As a result, Hignett was able to show the effect of almost the full range of behavior from zero to very strong rotation on the total heat transport by axisymmetric flow in a rotating annulus. His results are shown in Figure 1.20. The dependence of $\mathcal{N}$ and V on $\mathcal{P}$ in a rotating annulus subject to internal heating was also investigated by *Read* [1986], that also confirmed the above analysis provided the definition of $\mathcal{N}$ was modified appropriately to measure heat transport efficiency in terms of the temperature contrast obtained with a given heat flux; the results are shown in Figure 1.21. These clearly show the linear scaling of V with $\mathcal{P}$ in the weak rotation regime with a transition toward $\mathcal{P}^{1/2}$ as the moderate rotation regime is entered while the Péclet number also begins to reduce toward a $\mathcal{P}^{-1/2}$ dependence in the moderate rotation regime.

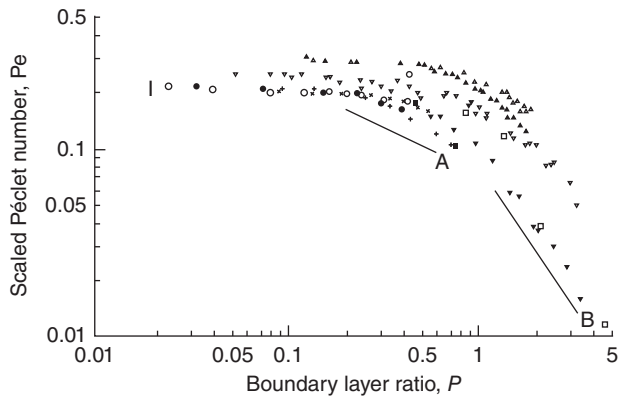

Figure 1.20. Scaled measurements of total heat transport in the axisymmetric regime of a rotating annulus as a function of $\mathcal{P}$. Adapted from *Hignett* [1982] by permission of Taylor & Francis Ltd., http://www.tandf.co.uk/journals.

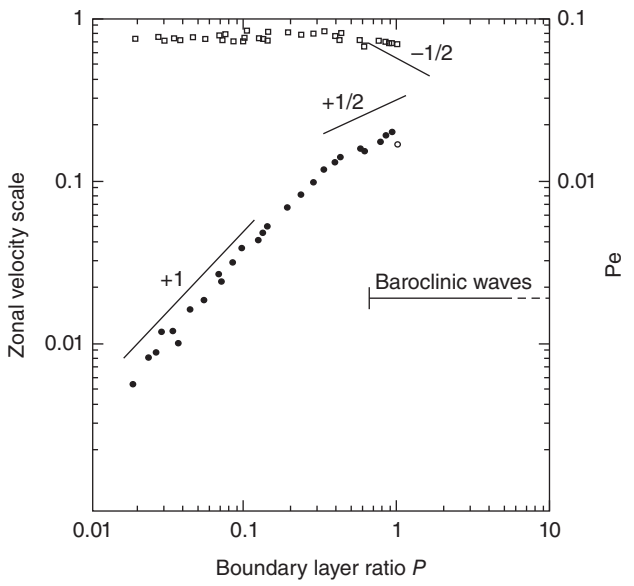

Figure 1.21. Schematic dependence of zonal (azimuthal) velocity scale on $\mathcal{P}$ in a rotating annulus subject to internal heating. Adapted from *Read* [1986] with permission.

1.4.3. Quantifying Baroclinic Eddy Transport

When baroclinic waves are not suppressed, as shown in Figure 1.18, heat transport evidently remains close to its nonrotating value as a result of eddy-induced transports. *Read* [2003] suggested that the latter can be viewed as adding to and enhancing the heat transport occurring in the axisymmetric boundary layer circulation, and the strength of this eddy-induced transport can therefore be diagnosed directly from measurements or simulations of total heat transport as the difference in Nusselt number between that of the fully three-dimensional flow and $\mathcal{N}$ obtained in a purely axisymmetric flow under the same experimental conditions. *Read* [2003] diagnosed this from a combination of numerical simulations of axisymmetric flows and experimental measurements. The results are shown in Figure 1.22, (a) as a function of both Ω and boundary layer ratio $\mathcal{P}$ and (b) as a function of the "supercriticality" of the flow defined with respect to a supercritical rotational Froude number $\mathcal{F}_s$, defined as

$$\mathcal{F}_s = \mathcal{F} - \mathcal{F}_{0m} = \frac{1}{\Theta} - \frac{1}{\Theta_{0m}}. \tag{1.57}$$

Here $\mathcal{F}$ is defined as $\mathcal{F} = 1/\Theta$ and $\Theta_{0m} = 1/\mathcal{F}_{0m}$ represents the critical values of Θ and $\mathcal{F}$ for the onset of baroclinic instability of azimuthal wave number m.

In this figure, the difference in Nusselt number represents an additional or "excess" Péclet number Pe_{xs} due to the presence of baroclinic waves. The effectiveness of baroclinic eddy heat transport grows rapidly with Ω from the first onset of baroclinic instability, rising to a value

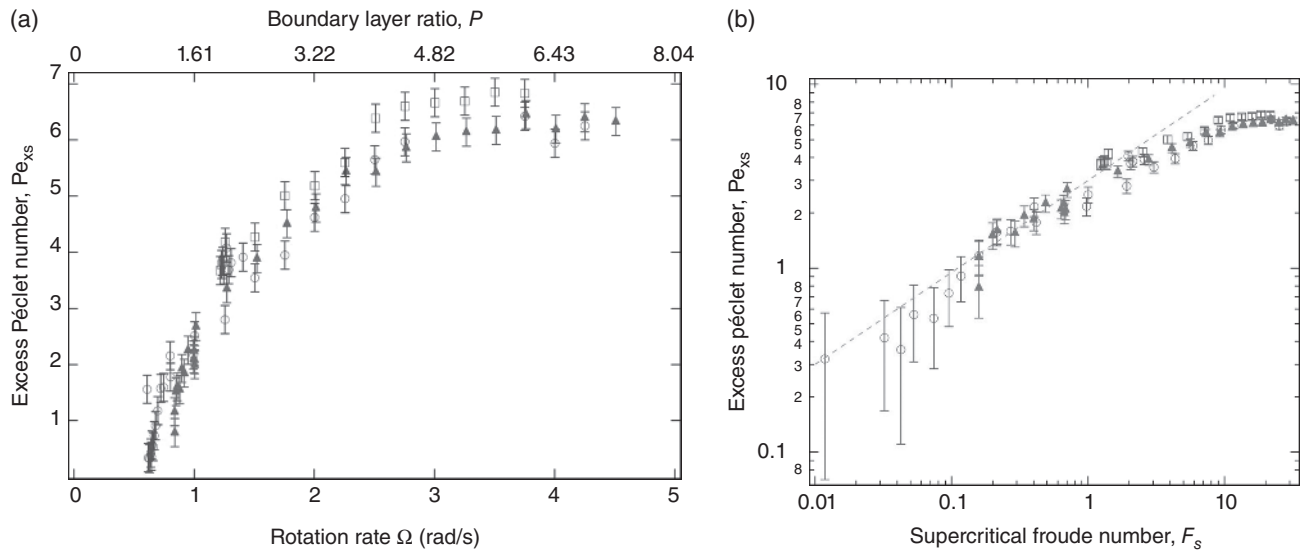

Figure 1.22. Experimental measurements of dimensionless integrated heat transport (excess Péclet number) attributable to baroclinic eddies in a rotating annulus experiment derived from data of *Read* [2003] and presented (a) as a function of Ω and $\mathcal{P}$ and (b) as a function of "supercritical" Froude number $\mathcal{F}_S$ (see text). Pe_{xs} may be compared with the nonrotating total Péclet number of around 10. Open circles are for $m = 2$ flows, filled triangles for $m = 3$, and open squares for $m = 4$ dominated flows. For color detail, please see color plate section.

(at least in the experiments discussed by *Read* [2003]) of around 6–7 at around $\Omega = 3$ rad/s, after which Pe_{xs} levels off and may even start to decrease at the highest values of Ω. This would appear to indicate that eddy-induced heat transport tends to saturate at a finite level once the instability becomes fully supercritical. Such an effect is also evident in Figure 1.22b, which shows the same data plotted against a measure of baroclinic supercriticality in terms of $\mathcal{F}_S$. This clearly indicates an initial dependence of Pe_{xs} close to $\mathcal{F}_S^{1/2}$ for $\mathcal{F}_S \lesssim O(1)$ (indicated by the dashed line in Figure 1.22b) but with a weaker dependence as $\mathcal{F}_S$ increases further. However, measurements penetrating further into the supercritical (irregular) regime would be desirable to confirm this saturation effect. The numerical simulations of *Pérez* [2006]; and *Pérez et al.* [2010] would seem to suggest that Pe_{xs} may continue to increase weakly as $\mathcal{P}$ is increased toward 10 (so the axisymmetric share of heat transport becomes relatively small), but these high Ω simulations probably had insufficient resolution to handle the increasingly turbulent wave flows at these high rotation rates, so the values of $\mathcal{N}$ may not represent accurately the heat transport of the real fluid system.

1.4.4. Testing Local Closures for Baroclinic Eddy Transport

Direct numerical simulations (DNSs), as discussed by *Pérez et al.* [2010], enable various diagnostics of complex baroclinic wave flows to be obtained that can be used to investigate quantitatively the validity of some of the assumptions underlying various approaches to eddy parameterization. *Read* [2003], *Pérez* [2006] and *Pérez et al.* [2010] have investigated various aspects of the diffusive approach to parameterizing heat transport in the context of the rotating annulus by making use of diagnostics of DNS model simulations of baroclinic annulus wave flows over a wide range of conditions with reference to the experimental measurements reported by *Read* [2003]. As mentioned above in the first part of this section, the notion that radial eddy heat flux should act down gradient with respect to its zonal mean field is implicit in various proposed parameterizations of eddy transport in the oceans and atmosphere, although this is notoriously difficult to deduce directly from theory or to verify in observations. However, many of these formulations are derived from simplified analyses based on quasi-geostrophic theory, so they should apply equally well to both geophysical situations and in the laboratory, at least within a limited range of parameters where quasi-geostrophy is reasonably valid.

Despite the well-established applicability of quasi-geostrophy to laboratory systems such as the rotating annulus [e.g., *Williams et al.*, 2010], however, there has been surprisingly little work done to investigate the parameterization of heat transfer in stably stratified flow in the laboratory and thereby to test the kinds of schemes proposed for use in models of oceans and atmospheres. In particular, *Pérez et al.* [2010] examined the extent to which baroclinic eddy fluxes of heat or vorticity (potential or

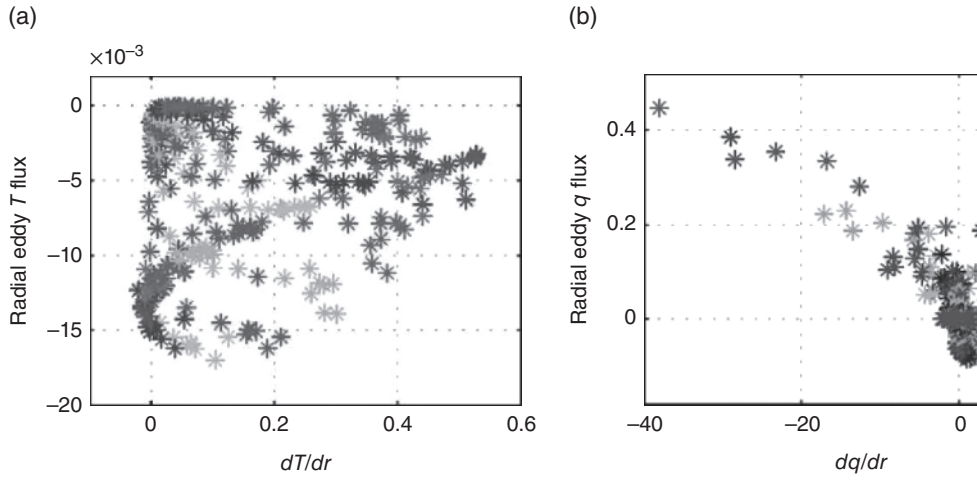

Figure 1.23. Scatter plots of eddy fluxes of heat and potential vorticity against their respective zonal mean gradient fields in numerical simulations by *Pérez* [2006]; and *Pérez et al.* [2010] of fully three-dimensional, time-dependent baroclinic waves flows under moderately supercritical conditions ($\Theta = 0.15$, $\mathcal{T} = 1.30 \times 10^7$). Plots were obtained by plotting pointwise values of fluxes and the respective radial gradient of the zonally averaged quantity across the whole meridional plane (outside boundary layers). (a) Correlation of meridional heat flux against zonal mean temperature gradient. (b) Corresponding correlation for eddy fluxes and zonal mean variations of QG potential vorticity. Adapted from *Pérez et al.* [2010]. Copyright 2010 with permission from Elsevier.

relative) act directly down-gradient with respect to various zonal mean fields in the simplest (right-cylindrical, axisymmetric annular channel with flat horizontal boundaries) configuration of the annulus experiment.

They found that, contrary to the commonly held assumption in many approaches that follow *Gent and McWilliams* [1990] (hereafter referred to as GM90), the horizontal eddy heat flux is only poorly correlated with the lateral gradient of zonal mean temperature. Figure 1.23a shows an example from Pérez et al.'s simulations in which the local eddy heat flux ($\overline{u'T'}$) is plotted against $\partial\overline{T}/\partial r$ in an equilibrated baroclinic wave flow under moderately super-critical conditions across the whole (r, z) plane of the annulus. Although some structure is evident, the dependence of ($\overline{u'T'}$) on $\partial\overline{T}/\partial r$ is clearly a lot more complicated than a simple, Fickian diffusive relationship would suggest. This appeared to be typical of most fully developed baroclinic wave simulations investigated by *Pérez et al.* [2010], with |correlation coefficients| $\lesssim 0.2$ in most cases except either under marginally unstable conditions or transiently during the initial growth of the instability, when correlation coefficients as large as -0.7 were found [*Pérez et al.*, 2010].

In contrast, fluxes of (potential or relative) vorticity were found to act quite closely down-gradient in most cases investigated. An example is shown in Figure 1.23b for quasi-geostrophic potential vorticity, plotted in the same way (and for the same case) as Figure 1.23a over the whole annular domain. In this case a strong anticorrelation is clearly evident, indicating that quasi-geostrophic potential vorticity is diffused horizontally by baroclinic eddies with respect to its zonal mean field to quite a good approximation. This behavior was found to be quite generic for almost all cases investigated, with correlation coefficients between $\overline{u'q'}$ and $\partial\overline{q}/\partial r$ ranging from -0.75 to -0.9 for both equilibrated and transient growing wave flows [*Pérez et al.*, 2010]. Similar behavior was also found for relative vorticity, in fact with even larger (negative) correlation coefficients than for potential vorticity.

Given such a clear correlation between eddy fluxes and mean gradients, *Pérez et al.* [2010] were able to deduce an effective eddy diffusivity $\mathcal{K}_q$ from a simple regression of ($\overline{u'q'}$) against $\partial\overline{q}/\partial r$ in their model simulations. A straightforward linear regression led to the remarkable result that $\mathcal{K}_q$ varied by less than a factor of 2 across the whole range of parameters investigated. Figure 1.24 shows the variation of the value of $\mathcal{K}_q$ obtained by *Pérez et al.* [2010] as a function of boundary layer ratio $\mathcal{P}$ (also cf Figure 1.18), indicating that, at least for these experiments, $\mathcal{K}_q$ was found to vary slowly between 1–2 $\times 10^{-2}$ cm^2/s. The largest values of $\mathcal{K}_q$ seemed to occur close to conditions of marginal instability, with $\mathcal{K}_q$ gradually reducing toward a roughly constant value $\sim 10^{-2}$ cm^2/s for all $\mathcal{P} \gtrsim 5$.

Given these results, *Pérez et al.* [2010] further tried to determine whether one or more previously proposed closures for $\mathcal{K}$ were sufficient to represent the variations found in their simulations based on an assumed form akin

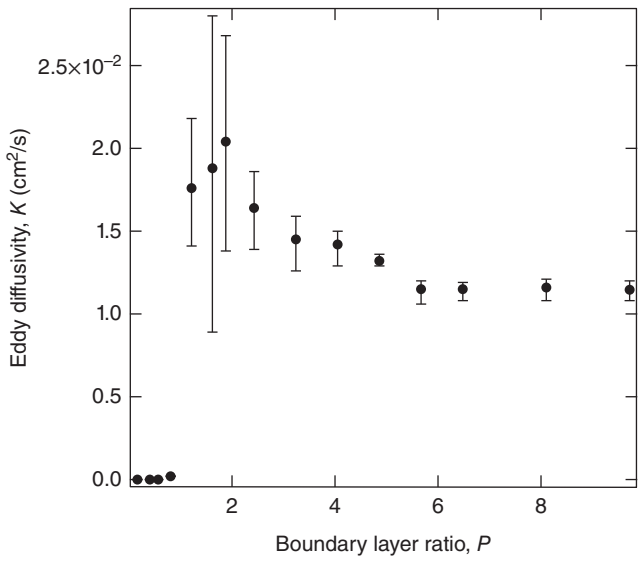

Figure 1.24. Dependence of eddy diffusivity for quasi-geostrophic potential vorticity on boundary layer ratio $\mathcal{P}$ (proportional to Ω) derived using data from correlating ($\overline{u'q'}$) against $\partial\overline{q}/\partial r$ in the rotating annulus model simulations of *Pérez et al.* [2010].

to equation (1.30) with L represented by the width of the baroclinic zone (i.e., the annulus gap width) and U_{eddy} given by a thermal wind scale

$$U_{\text{eddy}} \simeq \frac{LM^2}{N}, \tag{1.58}$$

where N is the Brunt-Väisäla frequency,

$$M^2 = \frac{g}{\overline{\rho}}\frac{\partial\overline{\rho}}{\partial r}, \tag{1.59}$$

such that $U_{\text{eddy}} \simeq 2\Omega L/\sqrt{\text{Ri}} \sim L/\tau_{\text{Eady}}$, τ_{Eady} is the linear growth time scale for the Eady model of baroclinic instability, and Ri is the characteristic shear Richardson number $\text{Ri} = N^2/(\partial u/\partial z)^2$ for the flow. In the event, no single closure seemed to apply across the whole parameter range. Such a result is not unduly surprising, since existing closures generally make assumptions based on either linear instability theory (which one might expect to hold close to marginal instability) or weakly nonlinear theory [e.g., *Pfeffer and Barcilon*, 1978]. Their results led to the conclusion that the observed variation of $\mathcal{K}_q$ with rotation was broadly consistent with weakly nonlinear theory close to conditions of marginal instability, with efficiency parameter α increasing roughly linearly with $\Theta - \Theta_c$ as suggested by *Pfeffer and Barcilon* [1978]. Under more strongly supercritical conditions, α appeared to converge to a roughly constant value that was consistent with the value obtained for example, by *Visbeck et al.* [1997], even to the extent of close quantitative agreement (0.013, cf. Visbeck et al.'s value of 0.015).

Thus, for strongly supercritical baroclinic flows, the annulus results obtained so far would seem to support a parameterization approach based on the potential vorticity diffusion hypothesis proposed by *Treguier et al.* [1997] (hereafter referred to as THL97) and *Killworth* [1997], with a closure for eddy diffusivity that is consistent with *Visbeck et al.* [1997]. Closer to marginal instability, however, a different closure would seem to be preferred that results in an increasing efficiency parameter α though not entirely following the simple, weakly nonlinear recipe of *Pfeffer and Barcilon* [1978]. Therefore, there would still seem, to be a number of unresolved issues underlying this somewhat unexpected behavior close to marginal instability. In addition, the approach of *Visbeck et al.* [1997] is overtly based on an application of linear instability theory in a regime that is far from where linear theory should be valid. The theoretical basis for this clearly deserves more attention in future work.

1.4.5. Implementing Eddy Parameterizations in an Annulus Model

The diagnostic approach discussed above using DNS is useful for investigating some of the underlying assumptions behind various approaches proposed for eddy transport parameterizations, especially those relating to the family of parameterizations following *Gent and McWilliams* [1990]. But in some respects the ultimate test of any given approach to this problem is actually to implement the parameterization in a numerical model. Although this has been common practice in generations of ocean circulation models for many years [e.g., *Danabasoglu et al.*, 1994], this is a relatively novel approach in the context of rotating annulus experiments and model simulations. Parameterizing turbulent transfers in rotating flows is, of course, of major importance for many engineering problems, e.g., in turbomachinery, where it has been customary for many years to employ large eddy simulation (LES) methods coupled with turbulence models based on rotational modifications to the classical Reynolds Averaged Navier-Stokes (RANS) model [e.g., see *Cazalbou et al.*, 2005, and references therein] to represent the effects of shear instabilities in the presence of background rotation. But the transformed Eulerian mean approach underlying the Gent-McWilliams family of parameterizations does not yet seem to have been adopted within the engineering community to represent unresolved eddy transports in stably stratified turbulence in rotating cavities.

Recently, however, *Pérez* [2006] has taken the first preliminary steps toward investigating this approach by implementing two forms of Gent-McWilliams parameterization in his 2D (axisymmetric), Boussinesq Navier-Stokes model of thermally driven flow in a fluid annulus

rotating at angular velocity Ω. As with his earlier diagnostic work, Perez's model was based on the conservative, finite-difference model described in detail by *Hignett et al.* [1985], which solves the full Boussinesq Navier-Stokes equations together with continuity and temperature advection-diffusion equations in cylindrical annular geometry using an exponentially stretched mesh in r and z to ensure adequate resolution of boundary layers. Nonslip, impermeable boundary conditions were applied at each boundary of the cavity, with fixed isothermal conditions at the inner and outer sidewalls and thermally insulating conditions on the horizontal boundaries. Fairly coarse resolution was adopted (32×32 points in (r, z)) in all cases. Each parameterized simulation was initialized from an isothermal state at rest in the rotating frame and then first run to equilibrium while holding the boundary conditions fixed. The eddy parameterization was then activated by adding parameterized vertical and radial velocity components $\mathbf{u}^*$, representing the transformed Eulerian mean (TEM) velocity field [e.g., *Andrews et al.*, 1987] induced by the presence of baroclinic eddies, to the 2D axisymmetric velocity field that was used to advect momentum and temperature, and the model was then integrated to its modified equilibrium.

The $\mathbf{u}^*$ parameterization was derived from the instantaneously computed velocity and temperature fields within the model either (a) using the original Gent-McWilliams method based on equations (1.25) and (1.27) or (b) derived from the zonal mean quasi-geostrophic potential vorticity field following THL97 based on equations (1.32) and (1.34). Because the zonally averaged isotherms become very steep as the sidewall boundary layers are approached, it was necessary to place limits on the isotherm gradient utilized in the eddy parameterization. *Pérez* [2006] used the method of *slope tapering* as advocated by *Danabasoglu and McWilliams* [1995] for use in ocean circulation models. This method was also used to control the PV gradients used in the THL97 parameterization, especially close to the boundaries of the domain. The closure used for $\mathcal{K}$ was either based on the formulation by *Visbeck et al.* [1997] or (for potential vorticity) a constant diffusivity equivalent to the value diagnosed from the fully 3D model simulations.

In practice, the original GM90 method was found to be capable of matching the total Nusselt number of the fully 3D simulated flows across the full range of parameters. However, apart from at the lowest rotation speeds (close to marginal instability), the resulting temperature fields did not match closely the zonally averaged fields obtained in the full 3D eddy-resolving model. This was almost certainly a reflection of the relatively weak correlation found by *Pérez et al.* [2010] between $(\overline{u'T'})$ and $\partial\overline{T}/\partial r$ in the full 3D flow, so that the parameterized eddy-induced circulation did not accurately reflect the real TEM circulation in the 3D flow. This actually led to the development of spurious numerical instabilities within the 2D parameterized model in the most strongly super critical simulations, even though the total heat transport of the 3D flow was reproduced quite accurately in most cases.

Although the alternative THL97 PV-based parameterization was not able to match the total Nusselt number of the full 3D simulations as accurately as the GM90 scheme, it did result in much more realistic zonally averaged temperature fields in the 2D parameterized model. Figure 1.25 shows examples of (a) the eddy-induced TEM stream function χ_q^*, (b) the resulting parameterized TEM radial velocity u^*, and (c) the eddy-induced TEM radial velocity diagnosed from the corresponding fully 3D, eddy-resolving model simulation at $(\Theta, \mathcal{T}) = (1.22, 1.6 \times 10^6)$. χ_q^* takes the form of a simple overturning aligned along the principal direction of the isotherms and in the sense required to advect them toward the horizontal. The corresponding parameterized u^* resembles the diagnosed TEM radial velocity quite closely except close to the boundaries of the domain, where isotherm and PV gradients in the main fields become very large and quasi-geostrophic theory is no longer valid.

Examples of some simulated temperature fields are shown in Figure 1.26, which shows (a) the zonally averaged equilibrated temperature field in (r, z) from a fully 3D eddy-resolving simulation of moderately supercritical flow at $(\Theta, \mathcal{T}) = (0.599, 3.26 \times 10^6)$, (b) the equilibrated temperature field from a 2D axisymmetric simulation under the same conditions as in (a), and (c) the corresponding equilibrated temperature field from a 2D simulation using the THL97 eddy parameterization implemented by *Pérez* [2006]. Under these conditions, the axisymmetric isotherms (b) are much more steeply sloped than obtained in the eddy-resolving 3D model (a), where fully developed baroclinic instability acts to release a lot of stored available potential energy. This is well reflected in the parameterized simulation, where the additional eddy-induced component of the meridional circulation has strengthened the advection of temperature sufficiently to relax the isotherm slope toward the horizontal in a way that emulates quite accurately the effects of baroclinic eddies on the zonal mean flow in the 3D eddy-resolving simulation, even to the point of retaining the static stability structure. The total Nusselt number in the parameterized simulation was 9.5 compared with a time-mean value of 10.1 in the 3D eddy-resolving simulation, indicating a tendency for parameterized simulations to underestimate eddy heat transfer by around 20%.

This tendency becomes more pronounced in more strongly supercritical conditions, with a parameterized Nusselt number of 7.5 compared with a 3D Nusselt number of 9.1 at the most extreme conditions investigated by *Pérez* [2006] at $(\Theta, \mathcal{T}) = (0.017, 1.17 \times 10^8)$. As remarked earlier, however, at these more extreme parameters the

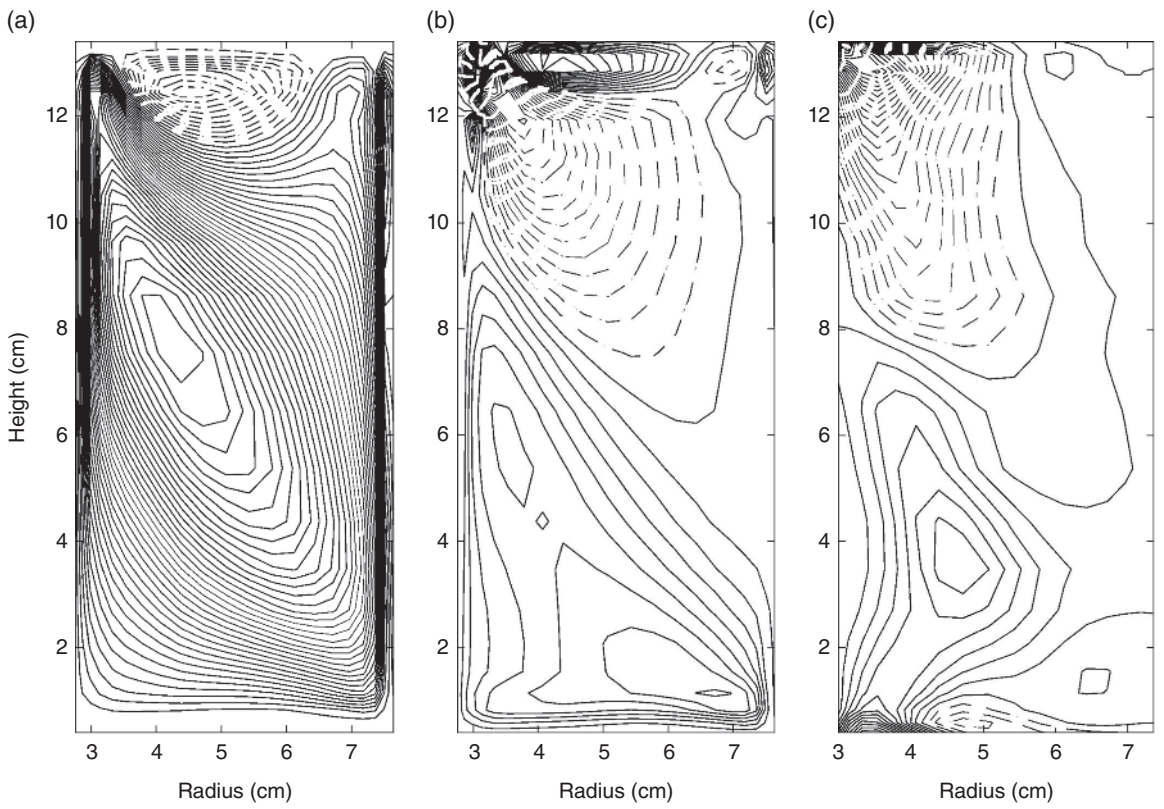

Figure 1.25. Maps in the (r, z) plane of (a) the eddy-induced transport stream function χ_q^* derived from a parameterization based on the zonal mean QG potential vorticity field [*Treguier et al.*, 1997], (b) the corresponding parameterized radial eddy-induced velocity ($u_* = 1/r\partial\chi_q^*/\partial z = (\mathcal{K}_q/f)\partial(\overline{q_{2D}})/\partial r$), and (c) radial eddy-induced velocity diagnosed from the fully 3D simulation ($u_* = -(\overline{u'q'})/f$) as obtained by *Pérez* [2006]. Note the remarkable degree of resemblance between (b) and (c). In each case negative values are shown with dashed contours.

simulated zonal mean temperature field begins to appear less obviously realistic, with apparent reversals of horizontal thermal gradient in the geostrophic interior, for example, that might reflect artifacts in the flow due to inadequate spatial resolution in the model. This needs to be investigated further in future work, which should include proper verification of the heat transfer and flow structure against laboratory measurements and the use of a higher resolution model.

1.5. DISCUSSION

In this chapter we have argued for the continued value and utility of rotating annulus laboratory experiments in the context of wider studies of the global circulation of planetary atmospheres and oceans. Despite many advances in the numerical modeling of atmospheres and oceans in the past 30 years, such approaches still have many limitations, particularly with regard to uncertainties associated with the use of finite resolution in space and time, the use of (often ad hoc) parameterization techniques to represent unresolved scales of motion, especially concerning the difficulty of accurately validating model simulations against measurements (which generally have incomplete and patchy coverage in space and time).

Laboratory studies help to focus attention on what factors may be fundamental to processes affecting the climate of an Earth-like planet, particularly under changing parametric conditions, in contrast to factors that may be incidental and/or specific to a particular system and may therefore be generalized across whole classes of system. The results presented above on quantifying heat transport in the thermally driven annulus system provide a prime example, in which we show how fundamental ideas on how the efficiency of heat transfer by baroclinic eddies appear to apply with equal validity both to laboratory flow systems and in the oceans (and in atmospheres too) provided the contribution to heat transfer in the laboratory due to the boundary layer circulation can be separated from that due to the baroclinic eddies themselves. This leads naturally to the use of laboratory experimental

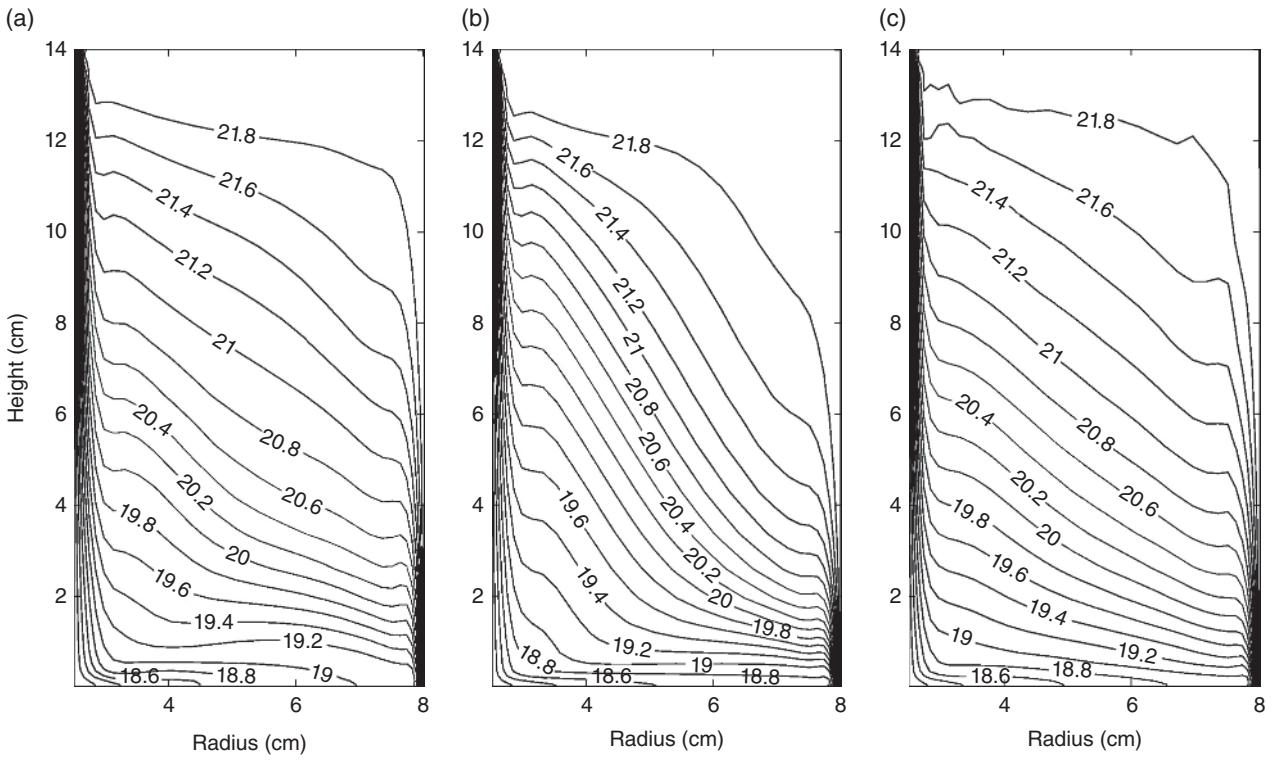

Figure 1.26. Maps in the (r, z) plane of (a) the zonal mean temperature field (in °C) derived from the equilibrated simulation using the 3D eddy-resolving numerical model (i.e., $\overline{T_{3D}}$), (b) the corresponding 2D axisymmetric temperature field T_{2D}, and (c) the equilibrated temperature field in a 2D axisymmetric model simulation using the THL97 eddy parameterization as obtained by *Pérez* [2006] for $\Delta T = 4$ K and $\Omega = 1.0$ rad/s ($\Theta = 0.599, \mathcal{T} = 3.26 \times 10^6$).

studies as rigorous means of testing theoretical hypotheses and understanding of heat transfer in geophysical problems.

A particular strength of the rotating annulus is its ability to achieve some degree of dynamical similarity with atmospheric and oceanic phenomena where background rotation is a dominating factor. In seeking to generalize results from the laboratory to geophysical systems, however, it is just as important to take account of the differences between experimental and natural systems as their similarities. The difference in geometry between cylindrical and spherical configurations is one obvious factor that must be taken into account, especially with regard to quantitative comparisons between experimental and geophysical systems. In addition, unlike in a planetary atmosphere or ocean, for example, diffusive boundary layers play major roles in the thermally driven annulus system in maintaining the mean stratification and horizontal thermal contrast in the quasi-geostrophic interior. This may make it difficult to use results from laboratory circulation systems to address mechanisms for setting the stratification in an ocean or atmosphere, for example, unless the experiment can be specifically reconfigured to reduce or allow for the influence of boundary layers.

The work described in Section 1.4 provides a powerful example of how combining insights and results from both real experiments and numerical model simulations can help to unravel the quantitative effects of boundary layer and quasi-geostrophic circulations within laboratory flows, thereby assisting in generalizing results from the latter to other systems. This methodological approach in intertwining laboratory measurements with numerical simulation offers the prospect of greatly increasing the scientific value of laboratory-based studies in the future

(a) by utilizing laboratory measurements to directly validate and compare numerical modeling techniques and to investigate e.g. convergence properties of model simulations with increasing resolution,

(b) by enabling simulations to be run that can test hypotheses under conditions (e.g., by artificially suppressing key instabilities) that may be difficult to realize directly in the laboratory, and

(c) ultimately to allow direct deterministic model predictions from initial states obtained using statistical-dynamical assimilation methods that combine model simulations with laboratory measurements.

The latter directly emulates the operational practice of numerical weather and climate prediction for Earth's

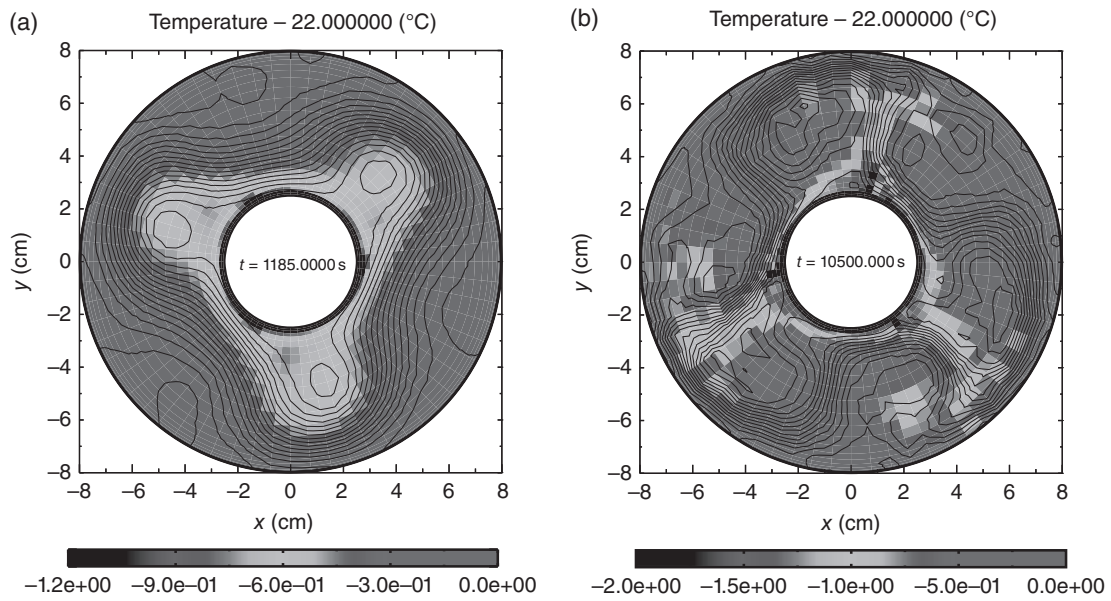

Figure 1.27. Representative temperature fields (colors) and horizontal stream function (contours) produced from assimilated horizontal velocity observations obtained in the same system as shown in Figures 1.8–1.13 and 1.21–1.26. Fields are plotted for regular (a) $\Omega = 0.875$ rad/s, $T_b - T_a \approx 4.07°$C) and chaotic flow (b) $\Omega = 3.1$ rad/s, $T_b - T_a \approx 4.02°$C) at $z = 9.7$ cm above the base of the annulus. Temperatures are relative to 22°C. Adapted from *Young and Read* [2013] with the permission of John Wiley & Sons, Inc. For color detail, please see color plate section.

atmosphere and oceans, offering the same potential uses to (a) obtain analyses of complete fields in the presence of incomplete and noisy measurements, (b) enable deterministic model predictions from assimilated measurements to quantify predictability and sensitivity to initial conditions, and (c) identify, characterize, and quantify systematic model errors.

The work by *Young and Read* [2013] applying data assimilation to the rotating annulus experiment in the form of analysis correction [*Lorenc et al.*, 1991] began to address some of these points. They demonstrated that it is possible to take methods developed for meteorological analysis and prediction and use them in the context of the laboratory experiment toward a useful end. In particular, they addressed the problem of incomplete measurements using the analysis correction procedure with a Boussinesq Navier-Stokes model to recover unobserved variables such as temperature (Figure 1.27) solely from irregularly distributed horizontal velocity observations at five vertical levels. The diagnostics required to shed light on the secondary instabilities at high rotation rate described in Section 1.3.4 were only obtainable because unobserved variables and vertically averaged quantities were retrieved via the assimilation procedure.

Although they did not address any outstanding problems with the analysis correction method itself (it has since been superseded by newer methods), this work laid the foundations to do so with newer methods not yet fully established in operational meteorological practice. Potential methods of interest include the various flavors of the ensemble Kalman filter (a version of which *Ravela et al.* [2010] have applied in this context) and other experimental methods that have been tested thus far primarily using low-dimensional systems [e.g., *Stemler and Judd*, 2009; *van Leeuwen*, 2010]. Laboratory experiments bridge the gap between these low dimensional systems and geophysical systems such as the atmosphere and, by using laboratory experiments, methods can be tested under laboratory conditions using a real fluid, a nonidealized model, and incomplete and noisy observations.

1.5.1. Planetary Circulation Regimes

An important question that still deserves a lot more attention than has been evident in the literature to date is the extent to which the rich and complex diversity of different flow regimes and bifurcations exhibited in the laboratory are shared, even qualitatively, by a full scale planetary atmosphere. The inability to carry out controlled experiments on real atmospheres is a major obstacle to progress in this regard (although of course such an approach would have other undesirable consequences for the inhabitants of such a planetary system!). The solar system provides a small sample of around eight planetary bodies with substantial atmospheres that occupy very different positions in parameter space. But this samples

the parameter space too sparsely to address the problem in much detail [e.g., see *Showman et al.*, 2010; *Read*, 2011, for reviews]. The growing number of discoveries of planets around other stars (e.g., see http://exoplanet.eu/ and *Schneider et al.* [2011]) offers the eventual prospect of sampling parameter space much more densely, but the available measurements are as yet much too crude to be able to provide quantitative characterization of circulation regimes. So at the present time (and for the foreseeable future) the only way of addressing and characterizing the diversity of planetary circulation regimes and bifurcations is through the use of numerical model simulations.

To date, however, relatively little has been done to define and sample an appropriate parameter space for planetary circulations that comes anywhere near matching what has been achieved in the laboratory, at least in terms of breadth and detail with respect to the dominant dimensionless parameters. The early work of *Geisler et al.* [1983] laid some of the foundations for this approach in using a stripped-down version of an atmospheric global circulation model (GCM) to investigate a range of prototypical circulations with an imposed equator-pole thermal contrast and varying rotation speeds of an Earth-like planetary atmosphere. By explicit analogy with laboratory rotating annulus experiments, they presented their results with respect to two dimensionless parameters:

(i) A thermal Rossby number defined as

$$\Theta_S = \left(\frac{gH}{f_0^2 L^2}\right)\frac{\Delta T}{T_r}, \tag{1.60}$$

where H is a pressure scale height ($= RT_r/g$), R is the gas constant, $f_0 = 2\Omega \sin\phi_0$ (ϕ_0 was taken to be a latitude of 45°), L is a horizontal length scale, ΔT is the imposed equator-pole temperature contrast at the surface, and T_r is a reference temperature.

(ii) A Taylor or inverse squared Ekman number, defined as

$$\mathcal{T} \simeq \mathcal{E}^{-2} = \frac{\Omega^2 H^4}{K_v^2}, \tag{1.61}$$

where K_v is a vertical "eddy viscosity" coefficient.

For various practical reasons *Geisler et al.* [1983] only studied cases equivalent to an Earth-like planet rotating at the same speed as or slower than Earth itself. But this did enable them to demonstrate the existence of a "lower symmetric" regime at relatively small ΔT, where wavy flows gave way to axisymmetric circulations, the boundary of which was found close to the line defined by $\Theta_S \simeq 10^5\mathcal{E}^2$. This roughly emulates the lower symmetric regime boundary found in rotating annulus experiments using relatively high Prandtl number fluids [*Fein*, 1973]. They also found evidence for a regular baroclinic wave regime at higher values of Θ_S than for Earth itself ($\Theta_S \gtrsim 0.05$), where the flow was dominated by near-monochromatic waves, peaking in amplitude at midlatitudes and drifting in longitude at a roughly steady rate. These waves were either steady in amplitude or apparently undergoing periodic oscillations reminiscent of the amplitude vacillation behavior seen in the annulus.

A significant difference from the laboratory systems was found, however, at the highest values of Θ_S, which would lie above the corresponding upper symmetric transition in the laboratory and would therefore be expected to exhibit axisymmetric flow. Instead, the flow in the spherical shell was found to transition from a predominantly baroclinic wave flow to a barotropically unstable flow, also with zonally propagating waves of relatively low zonal wave number $m \simeq 2$ drifting around an intense polar vortex. This kind of behavior has since been confirmed in more recent work [e.g., *Mitchell and Vallis*, 2010] in which such barotropically unstable flow at low planetary rotation speeds may also be associated with strongly superrotating zonal flow at low latitudes. Such a flow appears be consistent with the strongly superrotating circulations found on very slowly rotating planets such as Venus and Titan.

Since Geisler et al.'s early study, there has been a steady trickle of other work [e.g., *Williams and Holloway*, 1982; *Del Genio and Suozzo*, 1987; *Williams*, 1988a, 1988b; *Jenkins*, 1996; *Navarra and Boccaletti*, 2002; *Barry et al.*, 2002; *Schneider and Walker*, 2006] exploring other areas of parameter space, including cases corresponding to even faster rotation speeds (lower values of Θ_S) than Earth. Another early pioneer of this kind of modeling study was Gareth Williams [*Williams and Holloway*, 1982; *Williams*, 1988a, 1988b], who presented results from an Earth-like GCM for which the planetary rotation rate was varied between $\Omega_E/16$ and $\Omega_E \times 8$ (where Ω_E is Earth's rotation speed). At higher rotation speeds than that of Earth, Williams' model simulations suggested that the dominant scale of baroclinic instability would continue to decrease with increasing Ω, but with a tendency (at $\Omega \gtrsim 2\Omega_E$) for the subtropical zonal jet stream to break up into a set of two or more parallel jets associated with parallel trains of baroclinically unstable eddies. At the highest rotation speeds, up to seven or eight parallel jets were obtained in each hemisphere, resulting in a circulation pattern that bore a strong resemblance to that of Jupiter's or Saturn's cloud bands. Williams did not attempt to locate his simulations in a dimensionless parameter space, but *Read* [2011] computed approximate values of Θ_S and dissipation parameters to locate these experiments retrospectively. In common with some more recent work, the results appear to suggest that the multiple jets organize themselves on a scale comparable with the Rhines scale and are largely generated and controlled by the nonlinear interactions between eddies and the zonal flow.

This tendency to form multiple, parallel wave trains and zonal flows is reminiscent of the kind of flow regimes obtained in thermally driven annulus experiments with oppositely sloping end walls to generate a topographic β effect [e.g., *Mason*, 1975; *Bastin and Read*, 1997, 1998; *Wordsworth et al.*, 2008]. As argued by *Read* [2011], however, in contrast to laboratory experiments with boundaries of variable end wall slope, the global Rhines length scale ($\sim (U_{\rm rms}/\beta)^{1/2} \sim (U_{\rm rms} a/(2\Omega))^{1/2}$) is not independent of the thermal Rossby number in a planetary circulation. It is largely set by the spherical geometry and, in simple cases, may scale roughly as $\sqrt{\Theta_S}$ (though the full situation may be more complicated than this; e.g., see *Jansen and Ferrari* [2012] for further discussion). Thus, provided an analog of the planetary vorticity gradient is present in the laboratory, there appear to be strong parallels between the principal sequences of regime transitions in both cylindrical annular laboratory experiments and planetary atmospheres in spherical shells across much of the parameter space. But many gaps in our understanding of these parallels remain to be explored in detail.

However, the ability to run many experiments in the laboratory in order to sample parameter space densely offers the possibility of testing various theoretical scalings for circulations that operate on a planetary scale in atmospheres and oceans. Numerical models will continue to struggle to match this, especially at high planetary rotation rates where the range of dynamically significant scales of motion demands the use of very high resolution models.

Acknowledgments. Several aspects of this chapter originated in a series of graduate lectures given at the University of Oxford. It is a pleasure to thank the many colleagues and collaborators with whom I have worked on this problem for a number of years. Particular thanks are due to Drs. R. Hide, P. Hignett, M. J. Bell, and A. A. White of the UK Met. Office for their many insights and to D. W. Johnson, R. M. Small, W.-G. Früh, P. D. Williams, and A. A. Castrejón-Pita in connection with some of the experimental work discussed herein. We are also grateful to two anonymous referees whose comments greatly assisted in improving the presentation of this chapter.

REFERENCES

Abbe, C. (1907), Projections of the globe appropriate for laboratory methods of studying the general circulation of the atmosphere, *B. Am. Math. Soc.*, *13*, 502–506.

Andrews, D. G., J. R. Holton, and C. B. Leovy (1987), *Middle Atmosphere Dynamics*, Academic Press, Orlando, Fla.

Appleby, J. C. (1982), Comparative theoretical and experimental studies of baroclinic waves in a two-layer system, Ph.D. thesis, Univ. of Leeds.

Appleby, J. C. (1988), Selection of baroclinic waves, *Quart. J. R. Meteor. Soc.*, *114*, 1173–1179.

Baines, P. G. (1976), The stability of planetary waves on a sphere, *J. Fluid Mech.*, *73*, 193–213.

Barry, L., G. C. Craig, and J. Thuburn (2002), Poleward heat transport by the atmospheric heat engine, *Nature*, *415*, 774–777.

Basdevant, C., B. Legras, R. Sadourney, and M. Beland (1981), A study of barotropic model flows: Intermittency, waves and predictability, *J. Atmos. Sci.*, *38*, 2305–2326.

Bastin, M. E., and P. L. Read (1997), A laboratory study of baroclinic waves and turbulence in an internally heated rotating fluid annulus with sloping endwalls, *J. Fluid Mech.*, *339*, 173–198.

Bastin, M. E., and P. L. Read (1998), Experiments on the structure of baroclinic waves and zonal jets in an internally heated, rotating, cylinder of fluid, *Phys. Fluids*, *10*, 374–389.

Bell, M. J. (1989), Theoretical investigations prompted by experiments with baroclinic fluids, Ph.D. thesis, Imperial College London.

Bell, M. J., and A. A. White (1988), The stability of internal baroclinic jets: Some analytical results, *J. Atmos. Sci.*, *45*, 2571–2590.

Bernadet, P., A. Butet, M. Deque, M. Ghil, and R. Pfeffer (1990), Low-frequency oscillations in a rotating annulus with topography, *J. Atmos. Sci.*, *47*, 3023–3043.

Boville, B. A. (1981), Amplitude vacillation on a β-plane, *J. Atmos. Sci.*, *38*, 609–618.

Bowden, M. (1961), An experimental investigation of heat transfer in rotating fluids, Ph.D. thesis, Durham Univ., UK.

Bowden, M., and H. F. Eden (1965), Thermal convection in a rotating fluid annulus: Temperature, heat flow and flow field observations in the upper symmetric regime, *J. Atmos. Sci.*, *22*, 185–195.

Brachet, M. E., M. Meneguzzi, H. Politano, and P.-L. Sulem (1988), The dynamics of freely-decaying two-dimensional turbulence, *J. Fluid Mech.*, *194*, 333–349.

Brindley, J., and I. Moroz (1980), Lorenz attractor behaviour in a continuously stratified baroclinic fluid, *Phys. Lett.*, *77A*, 441–444.

Buzyna, G., R. L. Pfeffer, and R. Kung (1978), Cyclic variations of the imposed temperature contrast in a thermally driven rotating annulus of fluid, *J. Atmos. Sci.*, *35*, 859–881.

Buzyna, G., R. L. Pfeffer, and R. Kung (1984), Transition to geostrophic turbulence in a rotating differentially heated annulus of fluid, *J. Fluid Mech.*, *145*, 377–403.

Castrejón-Pita, A. A., and P. L. Read (2007), Baroclinic waves in an air-filled thermally driven rotating annulus, *Phys. Rev. E*, *75*, 026,301.

Cazalbou, J.-B., P. Chassaing, G. Dufour, and X. Carbonneau (2005), Two-equation modeling of turbulent rotating flows, *Phys. Fluids*, *17*, 055,110.

Charney, J. G., and M. E. Stern (1962), On the stability of internal baroclinic jets in a rotating atmosphere, *J. Atmos. Sci.*, *19*, 159–172.

Danabasoglu, G., and J. C. McWilliams (1995), Sensitivity of the global ocean circulation to parameterizations of mesoscale tracer transports, *J. Clim.*, *8*, 2967–2987.

Danabasoglu, G., J. C. McWilliams, and P. Gent (1994), The role of mesoscale tracer transports in the global ocean circulation, *Science*, *264*, 1123–1126.

Davies, T. V. (1959), On the forced motion due to heating of a deep rotating liquid in an annulus, *J. Fluid Mech.*, *5*, 593–621.

Del Genio, A., and R. J. Suozzo (1987), A comparative study of rapidly and slowly rotating circulation regimes in a terrestrial general circulation model, *J. Atmos. Sci.*, *44*, 973–986.

Drazin, P. G. (1970), Non-linear baroclinic instability of a continuous zonal flow, *Quart. J. R. Meteor. Soc.*, *96*, 667–676.

Drazin, P. G. (1978), Variations on a theme of eady, in *Rotating Fluids in Geophysics*, edited by P. H. Roberts and A. M. Soward, pp. 139–169, Academic Press, London and New York.

Esler, J. G., and B. T. Willcocks (2012), Nonlinear baroclinic equilibration at finite supercriticality, *Geophys. Astrophys. Fluid Dyn.*, *106*, 320–350.

Exner, F. M. (1923), Uber die bildung von windhosen und zyklonen, *Sitzungsber der Akad. der Wiss. Wien*, *Abt. IIa, 132*, 1–16.

Farmer, D., J. Hart, and P. Weidman (1982), A phase space analysis of baroclinic flow, *Phys. Lett.*, *91A*, 22–24.

Fein, J. (1973), An experimental study of the effects of the upper boundary condition on the thermal convection in a rotating cylindrical annulus of water, *Geophys. Fluid Dyn.*, *5*, 213–248.

Fein, J. S. (1978), *Boundary Layers in Homogeneous and Stratified-Rotating Fluids*, Univ. Presses of Florida, Tallahasee, Fla.

Fein, J. S., and R. L. Pfeffer (1976), An experimental study of the effects of prandtl number on thermal convection in a rotating, differentially heated cylindrical annulus of fluid, *J. Fluid Mech.*, *75*, 81–112.

Fjørtoft, R. (1953), On the changes in the spectral distribution of kinetic energy for two-dimensional nondivergent flow, *Tellus*, *5*, 225–230.

Fowler, A. C., J. D. Gibbon, and M. J. McGuinness (1982), The complex Lorenz equations, *Physica D*, *4*, 139–163.

Friedlander, S. (1980), *An Introduction to the Mathematical Theory of Geophysical Fluid Dynamics*, North Holland, Amsterdam, The Netherlands.

Früh, W. G., and P. L. Read (1997), Wave interactions and the transition to chaos of baroclinic waves in a thermally driven rotating annulus, *Phil. Trans. Roy. Soc. London*, *A355*, 101–153.

Fultz, D. (1951), Experimental analogies to atmospheric motions, in *Compendium of Meteorology*, edited by T. F. Malone, Am. Meteorol. Soc., New York.

Geisler, J. E., E. J. Pitcher, and R. C. Malone (1983), Rotating-fluid experiments with an atmospheric general circulation model, *J. Geophys. Res.*, *88*, 9706–9716.

Gent, P. R., and J. C. McWilliams (1990), Isopycnal mixing in ocean circulation models, *J. Phys. Oceanogr.*, *20*, 150–155.

Gent, P. R., J. Willebrand, T. J. Mcdougall, and J. C. McWilliams (1995), Parameterizing eddy-induced tracer transports in ocean circulation models, *J. Phys. Oceanogr.*, *25*, 463–474.

Gibbon, J. D., and M. J. McGuinness (1980), A derivation of the Lorenz equations for some unstable dispersive physical systems, *Phys. Lett.*, *77A*, 295–299.

Gill, A. E. (1966), The boundary-layer regime for convection in a rectangular cavity, *J. Fluid Mech.*, *26*, 515–536.

Green, J. S. A. (1970), Transfer properties of the large-scale eddies and the general circulation of the atmosphere, *Quart. J. R. Met. Soc.*, *96*, 157–185.

Grotjahn, R. (1984a), Baroclinic instability in a long wave environment. Part i. Review, *Quart. J. R. Meteor. Soc.*, *110*, 663–668.

Grotjahn, R. (1984b), Baroclinic instability in a long wave environment. Part ii. Ageostrophic energy conversions, *Quart. J. R. Meteor. Soc.*, *110*, 669–693.

Haine, T. W. N., and J. C. Marshall (1998), Gravitational, symmetric and baroclinic instability of the ocean mixed layer, *J. Phys. Oceanogr.*, *28*, 534–658.

Harlander, U., T. von Larcher, Y. Wang, and C. Egbers (2011), PIV- and LDV-measurements of baroclinic wave interactions in a thermally driven rotating annulus, *Exp. Fluids*, *51*, 37–49.

Hart, J. E. (1972), A laboratory study of baroclinic instability, *Geophys. Fluid Dyn.*, *3*, 181–209.

Hart, J. E. (1979), Finite amplitude baroclinic instability, *Ann. Rev. Fluid Mech.*, *11*, 147–172.

Hart, J. E. (1980), An experimental study of nonlinear baroclinic instability and mode selection in a large basin, *Dyn. Atmos. Oceans*, *4*, 115–135.

Hart, J. E. (1981), Wavenumber selection in nonlinear baroclinic instability, *J. Atmos. Sci.*, *38*, 400–408.

Hart, J. E. (1985), A laboratory study of baroclinic chaos on the f-plane, *Tellus*, *37A*, 286–296.

Hart, J. E. (1986), A model for the transition to baroclinic chaos, *Physica D*, *20*, 350–362.

Hide, R. (1958), An experimental study of thermal convection in a rotating fluid, *Phil. Trans. R. Soc. Lond.*, *A250*, 441–478.

Hide, R. (1970), Some laboratory experiments on free thermal convection in a rotating fluid subject to a horizontal temperature gradient and their relation to the theory of the global atmospheric circulation, in *The Global Circulation of the Atmosphere Joint Conference, 25–29 August 1969*, edited by G. A. Corby, Royal Meteorol. Soc., London.

Hide, R., and P. J. Mason (1970), Baroclinic waves in a rotating fluid subject to internal heating, *Phil. Trans. R. Soc. Lond.*, *A268*, 201–232.

Hide, R., and P. J. Mason (1975), Sloping convection in a rotating fluid, *Adv. Phys.*, *24*, 47–100.

Hide, R., P. J. Mason, and R. A. Plumb (1977), Thermal convection in a rotating fluid subject to a horizontal temperature gradient: Spatial and temporal characteristics of fully developed baroclinic waves, *J. Atmos. Sci.*, *34*, 930–950.

Hignett, P. (1982), A note on the heat transfer by the axisymmetric thermal convection in a rotating fluid annulus, *Geophys. Astrophys. Fluid Dyn.*, *19*, 293–299.

Hignett, P., A. Ibbetson, and P. D. Killworth (1981), On rotating thermal convection driven by non-uniform heating from below, *J. Fluid Mech.*, *109*, 161–187.

Hignett, P., A. A. White, R. D. Carter, W. D. N. Jackson, and R. M. Small (1985), A comparison of laboratory measurements and numerical simulations of baroclinic wave flows in a rotating cylindrical annulus, *Quart. J. R. Meteor. Soc.*, *111*, 131–154.

Hocking, L. M. (1978), Theory of hydrodynamic stability, in *Rotating Fluids in Geophysics*, edited by P. H. Roberts and A. M. Soward, pp. 437–469, Academic Press, London and New York.

Holopainen, E. O. (1961), On the effect of friction in baroclinic waves, *Tellus*, *13*, 363–367.

Holton, J. R. (1972), *An Introduction to Dynamic Meteorology*, Academic Press, New York.

Hoskins, B. J. (1973), Stability of the Rosby-Haurwitz wave, *Quart. J. R. Meteor. Soc.*, *99*, 723–745.

Hoskins, B. J. (1983), Dynamical processes in the atmosphere and the use of models, *Quart. J. R. Meteor. Soc.*, *109*, 1–21.

Hoskins, B. J., I. N. James, and G. H. White (1983), The shape, propagation and mean-flow interaction of large-scale weather systems, *J. Atmos. Sci.*, *40*, 1595–1612.

Jacoby, T. N. L., P. L. Read, P. D. Williams, and R. M. B. Young (2011), Generation of inertia-gravity waves in the rotating thermal annulus by a localised boundary layer instability, *Geophys. Astrophys. Fluid Dyn.*, *105*, 161–181.

James, I. N. (1994), *Introduction to Circulating Atmospheres*, Cambridge Univ. Press. Cambridge, UK.

Jansen, M., and R. Ferrari (2012), Macroturbulent equilibration in a thermally forced primitive equation system, *J. Phys. Oceanogr.*, *69*, 695–713.

Jenkins, G. S. (1996), A sensitivity study of changes in Earth's rotation rate with an atmospheric general circulation model, *Glob. Plan. Change*, *11*, 141–154.

Jnosi, I. M., P. Kiss, V. Homonnai, M. Pattantyús-Ábrahám, B. Gyüre, and T. Tél (2010), Dynamics of passive tracers in the atmosphere: Laboratory experiments and numerical tests with reanalysis wind fields, *Phys. Rev. E*, *82*, 046,308.

Killworth, P. D. (1997), On the parameterization of eddy transfer. Part I: Theory, *J. Mar. Res.*, *55*, 1171–1197.

Kim, K. (1978), Instability of baroclinic Rossby waves: Energetics in a two-layer ocean, *Deep Sea Res.*, *25*, 795–814.

King, E. M., S. Stellmach, J. Noir, U. Hansen, and J. M. Aurnou (2009), Boundary layer control of rotating convection systems, *Nature*, *457*, 301–304.

King, E. M., S. Stellmach, and J. M. Aurnou (2012), Heat transfer by rapidly rotating Rayleigh-Bénard convection, *J. Fluid Mech.*, *691*, 568–582.

King, J. C. (1979), Instabilities and nonlinear wave interactions in a two-layer rotating fluid, Ph.D. thesis, Univ. of Leeds.

Klein, P. (1990), Transition to chaos in unstable baroclinic systems: A review, *Fluid Dyn. Res.*, *5*, 235–254.

Kraichnan, R. H. (1967), Inertial ranges in two-dimensional turbulence, *Phys. Fluids*, *10*, 1417–1423.

Kraichnan, R. H. (1971), Inertial range transfer in two- and three-dimensional turbulence, *J. Fluid Mech.*, *47*, 525–535.

Larichev, V. D., and I. M. Held (1995), Eddy amplitudes and fluxes in a homogeneous model of fully developed baroclinic instability, *J. Atmos. Sci.*, *25*, 2285–2297.

Leach, H. (1981), Thermal convection in a rotating annulus: effects due to bottom topography, *J. Fluid Mech.*, *109*, 75–87.

Lewis, G. M., and W. Nagata (2004), Linear stability analysis for the differentially heated rotating annulus, *Geophys. Astrophys. Fluid Dyn.*, *98*, 129–152.

Li, G., R. Kung, and R. Pfeffer (1986), An experimental study of baroclinic flows with and without two-wave bottom topography, *J. Atmos. Sci.*, *43*, 2585–2599.

Lindzen, R. S., B. Farrell, and D. Jacqmin (1982), Vacillation due to wave interference: Applications to the atmosphere and to annulus experiments, *J. Atmos. Sci.*, *39*, 14–23.

Lorenc, A. C., R. S. Bell, and B. Macpherson (1991), The Meteorological Office analysis correction data assimilation scheme, *Q. J. Roy. Meteorol. Soc.*, *117*, 59–89.

Lorenz, E. N. (1963a), Deterministic non-periodic flow, *J. Atmos. Sci.*, *20*, 130–141.

Lorenz, E. N. (1963b), The mechanics of vacillation', *J. Atmos. Sci.*, *20*, 448–464.

Lorenz, E. N. (1967), *The Nature and Theory of the General Circulation of the Atmosphere*, No. 218, T. P. 115, World Metesral. Assoc., Geneva, Switzerland.

Lorenz, E. N. (1972), Barotropic instability of Rossby wave motion, *J. Atmos. Sci.*, *29*, 258–264.

Lovegrove, A. F. L., P. L. Read, and C. J. Richards (2000), Generation of inertia-gravity waves in a baroclinically unstable fluid, *Quart. J. R. Meteor. Soc.*, *126*, 3233–3254.

Lovegrove, A. F. L., I. M. Moroz, and P. L. Read (2001), Bifurcations and instabilities in rotating, two-layer fluids: I. f-plane, *Nonlin. Proc. Geophys.*, *8*, 21–36.

Lovegrove, A. F. L., I. M. Moroz, and P. L. Read (2002), Bifurcations and instabilities in rotating, two-layer fluids: Ii. β-plane, *Nonlin. Proc. Geophys.*, *9*, 289–309.

Marshall, D. P., and A. J. Adcroft (2010), Parameterization of ocean eddies: Potential vorticity mixing, energetics and Arnol'd's first stability theorem, *Ocean Modelling*, *32*, 188–204.

Mason, P. J. (1975), Baroclinic waves in a container with sloping endwalls, *Phil. Trans. Roy. Soc. London*, *278*, 397–445.

Maubert, P., and A. Randriamampianina (2002), Transition vers la turbulence géostrophique pour un écoulement d'air en cavité tournante différentiellement chauffée, *C. R. Méchanique*, *330*, 365–370.

McIntyre, M. E. (1968), The axisymmetric convective regime for a rigidly bounded rotating annulus, *J. Fluid Mech.*, *32*, 625–655.

McWilliams, J. C. (1984), The emergence of isolated coherent vortices in turbulent flow, *J. Fluid Mech.*, *146*, 21–43.

Mitchell, J. L., and G. K. Vallis (2010), The transition to superrotation in terrestrial atmospheres, *J. Geophys. Res.*, *115*, E12008.

Mundt, M. D., N. H. Brummell, and J. E. Hart (1995a), Linear and nonlinear baroclinic instability with rigid sidewalls, *J. Fluid Mech.*, *291*, 109–138.

Mundt, M. D., J. E. Hart, and D. R. Ohlsen (1995b), Symmetry, sidewalls, and the transition to chaos in baroclinic systems, *J. Fluid Mech.*, *300*, 311–338.

Navarra, A., and C. Boccaletti (2002), Numerical general circulation experiments of sensitivity to Earth rotation rate, *Climate Dyn.*, *19*, 467–483.

O'Gorman, P. A., and T. Schneider (2007), Recovery of atmospheric flow statistics in a general circulation model without nonlinear eddy-eddy interactions, *Geophys. Res. Lett.*, *34*, L2280.

Ohlsen, D. R., and J. E. Hart (1989a), The transition to baroclinic chaos on the β-plane, *J. Fluid Mech.*, *203*, 23–50.

Ohlsen, D. R., and J. E. Hart (1989b), Nonlinear interference vacillation, *Geophys. Astrophys. Fluid Dyn.*, *45*, 213–235.

Pedlosky, J. (1970), Finite-amplitude baroclinic waves, *J. Atmos. Sci.*, *27*, 15–30.

Pedlosky, J. (1971), Finite-amplitude baroclinic waves with small dissipation, *J. Atmos. Sci.*, *28*, 587–597.

Pedlosky, J. (1982a), Finite-amplitude baroclinic waves at minimum critical shear, *J. Atmos. Sci.*, *39*, 555–562.

Pedlosky, J. (1982b), A simple model for nonlinear critical layers in an unstable baroclinic waves, *J. Atmos. Sci.*, *39*, 2119–2127.

Pedlosky, J. (1987), *Geophysical Fluid Dynamics*, Springer, Berlin.

Pedlosky, J., and C. Frenzen (1980), Chaotic and periodic behavior of finite-amplitude baroclinic waves, *J. Atmos. Sci.*, *37*, 1177–1196.

Pérez, E. P. (2006), Heat transport by baroclinic eddies: Evaluating eddy parameterizations for numerical models, Ph.D. thesis, Univ. of Oxford.

Pérez, E. P., P. L. Read, and I. M. Moroz (2010), Assessing eddy parameterization schemes in a differentially heated rotating annulus experiment, *Ocean Modelling*, *32*, 118–131.

Pfeffer, R. L., and A. Barcilon (1978), Determination of eddy fluxes of heat and eddy temperature variances using weakly nonlinear theory, *J. Atmos. Sci.*, *35*, 2099–2110.

Pfeffer, R. L., G. Buzyna, and R. Kung (1980), Time dependent modes of behavior of thermally-driven rotating fluid, *J. Atmos. Sci.*, *37*, 2129–2149.

Phillips, N. A. (1954), Energy transformations and meridional circulation associated with simple baroclinic waves in a two-level quasi-geostrophic model, *Tellus*, *6*, 273–286.

Pierrehumbert, R. T. (2010), *Principles of Planetary Climate*, Cambridge Univ. Press, Cambridge, UK.

Plumb, R., and J. Mahlman (1987), The zonally-averaged transport characteristics of the GFDL general circualtion/transport model, *J. Atmos., Sci.*, *44*, 298–327.

Randriamampianina, A., W.-G. Früh, P. L. Read, and P. Maubert (2006), Direct numerical simulations of bifurcations in an air-filled rotating baroclinic annulus, *J. Fluid Mech.*, *561*, 359–389.

Ravela, S., J. Marshall, C. Hill, A. Wong, and S. Stransky (2010), A realtime observatory for laboratory simulation of planetary flows, *Exp. Fluids*, *48*, 915–925.

Read, P. L. (1986), Regimes of axisymmetric flow in an internally heated rotating fluid, *J. Fluid Mech.*, *168*, 255–289.

Read, P. L. (1988), On the scale of baroclinic instability in deep, compressible atmospheres, *Quart. J. R. Meteor. Soc.*, *114*, 421–437.

Read, P. L. (1992), Dynamics and instabilities of Ekman and Stewartson layers, in *Rotating Fluids in Geophysical and Industrial Applications*, edited by E. J. Hopfinger, pp. 49–84, Springer-Verlag, Vienna and New York.

Read, P. L. (2003), A combined laboratory and numerical study of heat transport by baroclinic eddies and axisymmetric flows, *J. Fluid Mech.*, *489*, 301–323.

Read, P. L. (2011), Dynamics and circulation regimes of terrestrial planets, *Plan. Space Sci.*, *59*, 900–914.

Read, P. L., and S. H. Risch (2011), A laboratory study of global-scale wave interactions in baroclinic flow with topography i: Multiple flow regimes, *Geophys. Astrophys. Fluid Dyn.*, *105*, 128–160.

Read, P. L., M. J. Bell, D. W. Johnson, and R. M. Small (1992), Quasi-periodic and chaotic flow regimes in a thermally driven, rotating fluid annulus, *J. Fluid Mech.*, *238*, 599–632.

Read, P. L., N. P. J. Thomas, and S. H. Risch (2000), An evaluation of Eulerian and semi-Lagrangian advection schemes in simulations of rotating, stratified flows in the laboratory. Part I: Axisymmetric flow, *Mon. Weather Rev.*, *128*, 2835–2852.

Rhines, P. B. (1979), Geostrophic turbulence, *Ann. Rev. Fluid Mech.*, *11*, 401–441.

Richardson, L. F. (1922), *Weather Prediction by Numerical Process*, Dover Publications, New York.

Romea, R. D. (1977), The effects of friction and β on finite amplitude baroclinic waves, *J. Atmos. Sci.*, *34*, 1689–1695.

Rossby, C. G. (1926), On the solution of problems of atmospheric motion by means of model experiments, *Mon. Weather Rev.*, *54*, 237–240.

Saffman, P. G. (1971), On the spectrum and decay of random two-dimensional vorticity distributions of large Reynolds number, *Stud. Appl. Math.*, *50*, 377–383.

Salmon, R. (1980), Baroclinic instability and geostrophic turbulence, *Geophys. Astrophys. Fluid Dyn.*, *15*, 167–211.

Salmon, R. S. (1978), Two-layer quasi-geostrophic turbulence in a simple special case, *Geophys. Astrophys. Fluid Dyn.*, *10*, 25–52.

Schneider, J., Dedieu, C., Le Sidaner, P., Savalle, R., and Zolotukhin, I. (2011), Defining and cataloging exoplanets: The exoplanet.eu database, *Astron. Astrophys.*, *532*, A79. doi:10.1051/0004-6361/201116713.

Schneider, T., and C. C. Walker (2006), Self-organization of atmospheric macroturbulence into critical states of weak nonlinear eddy-eddy interactions, *J. Atmos. Sci.*, *63*, 1569–1586.

Scott, R. B., and B. K. Arbic (2007), Spectral energy fluxes in geostrophic turbulence: Implications for ocean energetics, *J. Phys. Oceanogr.*, *37*, 673–688.

Scott, R. B., and F. Wang (2005), Direct evidence of an oceanic inverse energy cascade from satellite altimetry, *J. Phys. Oceanogr.*, *35*, 1650–1666.

Showman, A. P., J. Cho, and K. Menou (2010), Atmospheric circulation of extrasolar planets, in *Exoplanets*, edited by S. Seager, pp. 471–516, Univ. of Arizona Press, Tueson, Ariz.

Sitte, B., and C. Egbers (2000), Higher order dynamics of baroclinic waves, in *Physics of Rotating Fluids. Proc. 11th Int. Couette-Taylor Workshop, July 20–23, 1999, Bremen, Germany*. C. Egbers and G. Pfister (Eds), LNP 549, pp. 355–375. Springer-Verlag, Berlin & Heidelberg.

Spence, T. W., and D. Fultz (1977), Experiments on wave-transition spectra and vacillation in an open rotating cylinder, *J. Atmos. Sci.*, *34*, 1261–1285.

Stemler, T., and K. Judd (2009), A guide to using shadowing filters for forecasting and state estimation, *Phys. D*, *238*, 1260–1273.

Stone, P. (1972), A simplified radiative-dynamical model for the static stability of rotating atmospheres, *J. Atmos. Sci.*, *29*, 405–418.

Sugata, S., and S. Yoden (1992), Steady axisymmetric flow due to differential heating in a rotating annulus and its dependence on experimental parameters, *J. Met. Soc. Japan*, *70*, 1005–1017.

Sugata, S., and S. Yoden (1994), Chaotic Lagrangian motion and heat transport in a steady, baroclinic annulus wave, *J. Met. Soc. Japan*, *72*, 569–587.

Tajima, T., T. Nakamura, and T. Kuroda (1995), Laboratory experiments of Lagrangian motions in a steady baroclinic wave - internal structures of vortices, *J. Met. Soc. Japan*, *73*, 37–46.

Tajima, T., T. Nakamura, and K. Kurosawa (1999), Experimental observations of 3D Lagrangian motions in steady baroclinic waves: II, *J. Met. Soc. Japan*, *77*, 17–29.

Tamaki, K., and K. Ukaji (2003), An experimental study of wave dispersion in a differentially heated rotating fluid annulus with a radially sloping bottom, *J. Met. Soc. Japan*, *81*, 951–962.

Treguier, A. M., I. M. Held, and V. D. Larichev (1997), Parametrization of quasigeostrophic eddies in primitive equation ocean models, *J. Phys. Oceanogr.*, *27*, 567–580.

Ukaji, K., and K. Tamaki (1989), A comparison of laboratory experiments and numerical simulations of steady baroclinic waves produced in a differentially heated rotating annulus, *J. Met. Soc. Japan*, *67*, 359–373.

Vallis, G. K. (2006), *Atmospheric and Oceanic Fluid Dynamics: Fundamentals and Large-Scale Circulation*, Cambridge Univ. Press, Cambridge, UK.

van Leeuwen, P. J. (2010), Nonlinear data assimilation in geosciences: An extremely efficient particle filter, *Q. J. Roy. Meteorol. Soc.*, *136*, 1991–1999.

Vettin, F. (1857), Uber den aufsteigen Luftström, die Entstehung des Hagels und der Wirbel-Stürme, *Ann. Physik Chemie*, *102*, 246–255.

Vettin, F. (1884), Experimentale darstellung von luftbewegungen unter dem einflusse von temperatur-unterschieden und rotations-impulsen, *Meteorolol. Z.*, *1*, 227–230, 271–276.

Visbeck, M. J., J. Marshall, and T. W. N. Haine (1997), Specification of eddy transfer coefficients in coarse-resolution ocean circulation models, *J. Phys. Oceanogr.*, *27*, 381–402.

von Larcher, T., and C. Egbers (2005), Experiments on transitions of baroclinic waves in a differentially heated rotating annulus, *Nonlin. Proc. Geophys.*, *12*, 1033–1041.

von Larcher, T., A. Fournier, and R. Hollerbach (2013), The influence of a sloping bottom endwall on the linear stability in the thermally driven rotating annulus with a free surface, *Theor. Comput. Fluid Dyn.*, 27, 433–451.

Warn, T., and P. Gauthier (1989), Potential vorticity mixing by marginally unstable baroclinic disturbances, *Tellus*, *41A*, 115–131.

Weng, H.-Y., and A. Barcilon (1987), Wave structure and evolution in baroclinic flow regimes, *Quart. J. R. Meteor. Soc.*, *113*, 1271–1294.

Weng, H.-Y., A. Barcilon, and J. Magnan (1986), Transitions between baroclinic flow regimes, *J. Atmos. Sci.*, *43*, 1760–1777.

White, A. A. (1988), The dynamics of rotating fluids: numerical modelling of annulus flows, *Met. Mag.*, *117*, 54–63.

White, H. D., and E. L. Koschmieder (1981), Convection in a rotating, laterally heated annulus. Pattern velocities and amplitude oscillations, *Geophys. Astrophys. Fluid Dyn.*, *18*, 301–320.

Willcocks, B. T., and J. G. Esler (2012), Nonlinear baroclinic equilibration in the presence of Ekman friction, *J. Phys. Oceanogr.*, *42*, 225–242.

Williams, G. P. (1988a), The dynamical range of global circulations. I, *Clim. Dyn.*, *2*, 205–260.

Williams, G. P. (1988b), The dynamical range of global circulations. II, *Clim. Dyn.*, *3*, 45–84.

Williams, G. P., and J. L. Holloway (1982), The range and unity of planetary circulations, *Nature*, *297*, 295–299.

Williams, P. D., T. W. N. Haine, and P. L. Read (2005), On the generation mechanisms of short-scale unbalanced modes in rotating two-layer flows with vertical shear, *J. Fluid Mech.*, *528*, 1–22.

Williams, P. D., T. W. N. Haine, and P. L. Read (2008), Inertia-gravity waves emitted from balanced flow: Observations, properties, and consequences, *J. Atmos. Sci.*, *65*, 3543–3556.

Williams, P. D., P. L. Read, and T. W. N. Haine (2010), Testing the limits of quasi-geostrophic theory: Application to observed laboratory flows outside the quasi-geostrophic regime, *J. Fluid Mech.*, *649*, 187–203.

Wordsworth, R. D., P. L. Read, and Y. H. Yamazaki (2008), Turbulence, waves, and jets in a differentially heated rotating annulus experiment, *Phys. Fluids*, *20*, 126,602.

Young, R. M. B., and P. L. Read (2008), Flow transitions resembling bifurcations of the logistic map in simulations of the baroclinic rotating annulus, *Physica D*, *237*, 2251–2262.

Young, R. M. B., and P. L. Read (2013), Data assimilation in the laboratory using a rotating annulus experiment, *Quart. J. R. Meteor. Soc.*, p. in press.

Zurita-Gotor, P., and R. S. Lindzen (2007), Theories of baroclinic adjustment and eddy equilibrations, in *The Global Circulation of the Atmosphere*, edited by T. Schneider and A. H. Sobel, pp. 22–46, Princeton University Press, Princeton, N.I.